

Portia Bryce
Dante Bagnasco
Samantha Schmid
Austin Burns
Tristan Burchfield
Jacob Bryce

November 23, 2025
MAE 489: Erik Andersen

Full Capstone Report: Group 1- LiDAR

Executive Summary

Autonomous vehicles are beginning to operate on public roads, but their reliability is limited by poor visibility in weather conditions such as rain, snow, and fog. Current systems rely heavily on LiDAR and camera-based perception to detect street signs and lane markings. When visibility is limited, LiDAR performance decreases, forcing autonomous vehicles to operate only in clear-weather regions. This project is focused on the design and testing of a radar-enhanced street sign that produces a strong, repeatable radar signature, allowing a vehicle to determine its position relative to the sign using radar when LiDAR is impaired.

The team first used user and expert interviews to create design specifications focused on safety, accuracy, reliability, and cost. Key metrics included maintaining >90% detection accuracy in bad weather and achieving localization within 0.5 m (1.6 feet) of true sign position. A brainstorming process generated more than twenty concepts, including heated traditional signs, Doppler radar systems, ultrasonic sonar, and vehicle-to-vehicle communication. These ideas were evaluated with a weighted decision matrix, emphasizing weather adaptability, reliability, simplicity, power requirements, and cost. The hollow radar sign scored the highest overall because it is passive (no power needed), compatible with existing roadside infrastructure, and scalable for mass deployment.

The resulting prototype is a steel street sign with a hollow internal cavity and a modified front face. The original single-square opening was reworked by adding a plate to create two narrower openings, encouraging internal scattering of radio waves and producing a more distinct “double peak” in the radar graph. The sign is mounted on a steel stand, similar to standard sign posts. For testing, the team used a Texas Instruments AWR1642 radar and an Intel RealSense LiDAR, along with a fog machine, snow machine, and rain simulator. Control and weather tests were performed at distances of 10, 15, and 20 feet, and at angles from -30° to +30°, with multiple trials at each condition. The data was analyzed using mean values, 95% confidence intervals, and percent error in measured distance.

Results show that the hollow sign provides a robust and readable radar signature across the tested distances and weather conditions. In clear (control) tests, the radar’s distance estimates

were within about 1-5% of the true distance over the 10-20 foot range, indicating consistent and accurate localization. When snow, rain, and fog were introduced, the sign continued to produce the same distinctive two-peak radar pattern. The first peak stayed within 0.1-1.3 feet of the true distance, while the second peak stayed within 0.4-2 feet. Peak magnitudes in adverse weather remained strong, with first peak values in the 97-115 dB range (for example, around 108 dB in snow at 15 feet), providing a large detection margin even when visibility would be poor for human drivers. Angular offers up to $\pm 30^\circ$ reduced peak magnitudes by about 10-20 dB, but distance errors remained under 0.8 feet, showing that angle primarily affects signal strength rather than distance estimation. Overall, these results suggest that the prototype meets the projected goals of providing a stable radar signature in low-visibility environments and can support autonomous vehicle function when LiDAR is impaired.

Comparative LiDAR tests showed the need for radar-based infrastructure. In the same weather conditions, LiDAR could not reliably detect the sign. The data confirmed that a hollow street sign can maintain a strong, distinctive radar signature and localization accuracy in weather conditions where LiDAR fails. This proof of concept suggests that radar-based street signs could improve the safety and reliability of autonomous vehicles as they expand into regions with rain, snow, and fog.

Introduction

Autonomous vehicles have begun to roll out in waves, with companies like Waymo, Cruise, Tesla, and Nuro being the primary providers for public use. Waymo has the highest level of automation, being level 4 out of 5, allowing the vehicle to perform all driving tasks under specific circumstances, with human interactions still being a possibility [4]. Therefore, the car relies heavily on LiDAR and radar sensors for its position, speed, and distance from other objects on the road [14]. LiDAR uses pulses of laser light to measure distances and shapes of objects to create a 3D digital model. A series of images can be used to create an environment around the car. This functionality is intuitive because human eyes use a similar mechanism.

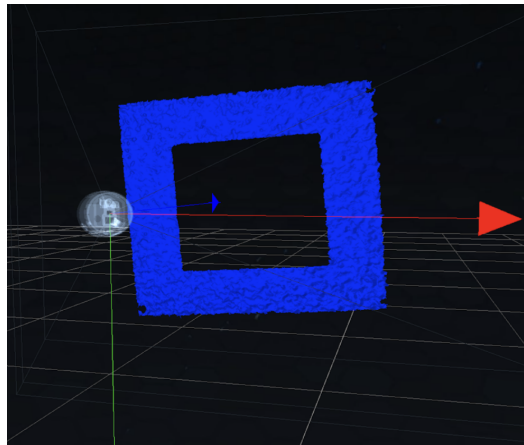


Figure 1. LiDAR image of a square plate with a hole.

When air clarity is disturbed by rain, snow, or fog, LiDAR functionality decreases dramatically. It cannot capture information from street signs, road markings, or surrounding vehicles. Waymo's are stationed in Arizona and California for their traditionally clear skies. Looking forward, it can be expected that autonomous vehicles will spread nationally. Managing ineffective LiDAR will become critical for implementation in colder climates.

Radar may be able to fill this gap because it travels through disorder easier than LiDAR does. Radar uses radio waves to send and receive signals to interpret and categorize distance, direction, and speed. It can be a location tool for cars when LiDAR systems are handicapped by weather. Positioning with radar is more difficult because its output is a 2D graph of distance vs. power which is less intuitive and gives fewer data points than LiDAR does.

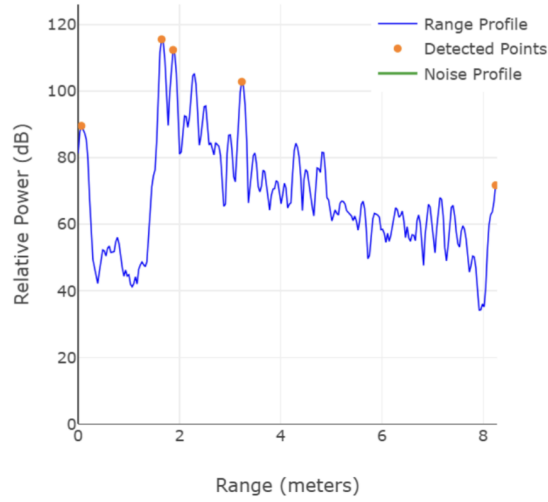


Figure 2. Example of radar output with range (meters) on the x-axis and Relative Power (dB) on the y-axis

In a scenario where LiDAR is deemed ineffective, can radar alone locate a vehicle under the same conditions? In solving this, it is necessary to make a system which can trigger a unique, repeatable, and informative reading from the radar. This project utilizes a patented street sign with a hollow cavity (Fig. 3) to produce a unique signature by reflecting the radar waves internally (Fig 2.). It investigates the reliability of these readings and the data that can be obtained. The goal is to find a car's relative position to a sign solely through radar images and verify its accuracy in bad weather.

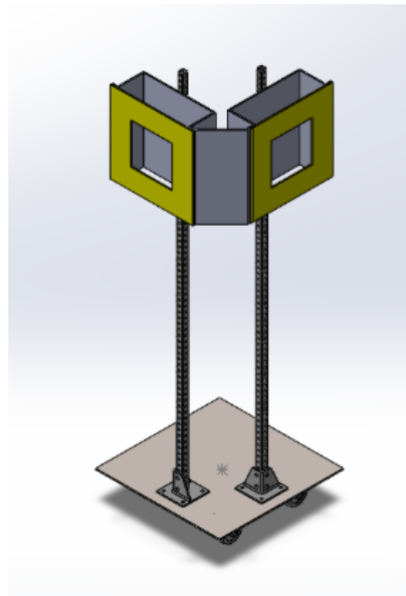


Figure 3. Street sign with hollow cavity for testing

The broader impact of this product lies in improving the safety and reliability of autonomous vehicles in all weather conditions. Currently, limited visibility in snow, rain, and fog is one of the most significant barriers to widespread adoption of autonomous vehicles. By introducing street signs with engineered cavity geometries, roadway infrastructure can actively support vehicle perception systems rather than relying solely on onboard sensors. This increases the ability of AVs to navigate themselves in poor conditions, reducing the risk of collisions and improving passenger confidence in the technology.

Currently, self-driving vehicles struggle with poor visibility conditions. They use LiDAR and Radar sensors, which are better than normal cameras which only see visible light. They cannot read existing street signs when the normal cameras are impaired.

**Waymo Driver's
superhuman sensing ability**

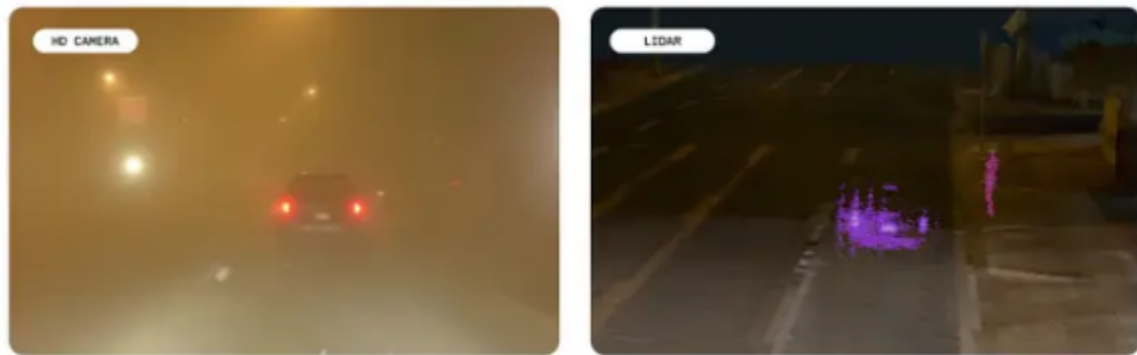


Figure 4. Waymo LiDAR sensor seeing a person in a dust storm vs what a normal camera sees

By making new street signs with cavities, radar sensors would be able to “see” our sign in poor weather conditions. The sign geometry can be modified to give several signatures. The car can recognize these as current street sign variations. This technology is still hypothetical and needs further testing to be proved. This research is focused on a proof of concept rather than the implementation of the sign.

Also, solutions such as this can create a standardized approach for transportation agencies as autonomous vehicles expand regions like Arizona and California. A national system of signage could support economic growth in the AV sector. Ultimately, the product represents not only a technical advancement in sensor integration but also a step toward safer roads and greater public trust in emerging autonomous systems.

Products that Use Self Driving Capabilities:

Tesla: Tesla's current technology for self driving and assisted driving mainly utilizes cameras instead of LiDAR and Radar [10]. Tesla currently is working on automotive taxi's similar to waymo, but in their current vehicles, it is rated at a level 2 autonomy. This means the vehicles still require piloted guidance from someone inside the vehicle. This technology has been proven useful in the correct circumstance, but according to their drivers manual, it still struggles with complex road conditions such as constructions as well as poor visibility due to harsh weather conditions [12].

Cruise: Cruise is the self driving technology from general motors that utilizes LiDAR and Radar. They currently have a level 2 autonomy system and are in the testing periods for a level 3 system [9]. A recent accident with a Cruise vehicle highlighted the limitations of this technology. The accident wasn't directly caused by harsh weather conditions, but the cars visual capabilities were questioned due to the accident, leading to concerns with driving in harsher conditions [7].

Waymo: Waymo is currently the highest level of autonomous vehicle at autonomy level 4. They utilize LiDAR, Radar and cameras in unison for a driverless experience [14]. While it is the most advanced out of the options currently available, harsh weather conditions and complex road conditions cause the car confusion [2].

Methods

The team conducted a series of interviews with both users and technical experts relating to autonomous vehicles (AV) to gather further understanding about the performance, expectations, and challenges associated with AV systems. With a specific insight into the integration of LiDAR and Radar technologies. Two users, Cadence Mullens and Adam Frazier, were interviewed as they were both owners of Tesla vehicles with self-driving capabilities, to obtain valuable feedback based on their experience with their experiences and limitations.

Cadence Mullens reports that using Tesla's autonomous features intermittently for two months. She stated several issues, including difficulty detecting old or faded lane markings, misreading of yellow lights, and the failure to recognize new or temporary signage, such as construction or school zones. She also noted that the system performed poorly in heavy rain but worked well in clear weather conditions and at night. Her main concern presented was safety, emphasizing that having redundant systems of LiDAR and Radar would improve reliability and user confidence.

Adam Frazier had two years of consistent use of Tesla's self-driving system and occasional use of Waymo vehicles around Arizona. He has observed that Tesla's systems were more robust; meanwhile, Waymo's often struggled with irregular patterns in the road. Some examples include construction zones, school zones, and other changes to the road that aren't normal; oftentimes, these areas will require human intervention to maneuver around the obstruction. He also emphasizes that they do not perform testing in varied weather conditions, limiting their real-world reliability. Similar to Cadence, he highlighted safety, obstacle avoidance, and lane-keeping as the most critical functions and therefore supported the idea of multiple redundancies to help maneuver the vehicle.

Overall, both users identify safety, reliability, and environmental adaptability as top priorities. They agreed that autonomous systems need to improve before being applied to other states with different road conditions, weather conditions, and external road conditions. They both agreed that the more redundancy in sensing (Radar and LiDAR systems) would enhance user trust. Two experts were also interviewed: Jeff Bryce and Christine Schmid, providing technical insights on sensor design, project execution, and system optimization.

Jeff Bryce, who initially conceptualized the LiDAR/Radar street sign project in 2021, emphasized the importance of project management, documentation, and early testing. He advised the team to make documentation of every process and result to ensure repeatability and traceability during sensor setup and data collection. He also stressed comparing the team's findings to pre-existing AV sensors to validate improvements. Jeff provided information that frequency, sample rate, and environmental testing (fog, rain, and snow) are crucial to proving the reliability of LiDAR and Radar systems in real-world applications, in how they succeed and fail.

Christine Schmid, an electrical engineer who specializes in control systems and aerospace applications, provided an in-depth understanding of LiDAR and Radar functionality. She explained that LiDAR generates high-resolution 3D terrain maps using laser pulses, making it excellent for precision navigation and obstacle avoidance, but highly dependent on the weather conditions. Meanwhile, Radar uses radio waves that provide reliability in poor visibility conditions but with lower resolution, as it is similar to points on a map rather than a 3D map. According to Schmid, combining LiDAR and Radar systems counteracts each system's limitations, providing both accuracy and reliability to improve in obstacle detection, terrain mapping, and navigation safety.

User Needs

The user needs testing aimed at placing the design team in the position of potential users and understanding how they might interact with or depend on the LiDAR/Radar to function with the street sign. This process helped to identify how users perceive the sign and what limitations could be present in the current AV systems, and how the new sign could enhance the vehicle's performance in poorer weather conditions. The team's research focused on existing literature and technical data concerning LiDAR and Radar use in AV. We analyzed limitations in resolution, frequency, field of view, and environmental adaptability to better define user expectations.

The first key finding was that safety is the most important priority; the safety of the passengers, pedestrians, and surroundings of the vehicles is the number one priority. Any AV enhancement should reduce the risk of accidents, especially in unpredictable environments. The second highest being the environmental reliability, the system must perform dependably under a variety of weather conditions, rain, fog, or snow, which can be seen as nonideal when compared to clear weather conditions. An integration with maps should apply to pre-existing systems that are already in place, such as Google Maps, Apple Maps, etc., to be efficient navigation, but also be able to function independently if mapping is unavailable. This system should be affordable; the LiDAR and Radar systems are already applied to most high-end AV, such as Waymo, but the street signs must be economically viable for large-scale implementations by cities and vehicle manufacturers to be a "valid" solution. The last key point should be that the system should be able to respond to temporary road closures, such as constructions or detours, with minimal human interaction.

Based on both the interview data and user needs testing, the following list summarizes the essential requirements identified for the LiDAR/Radar street sign project.

Table 1. User Needs Analysis

| User Needs | Explanation | Priority |
|---|---|--------------|
| 1. Safety in AV, even in poor weather conditions. | Safety is the highest concern for all users and experts. The system must reduce accident risk and maintain control in varying environmental conditions. | Critical (1) |
| 2. Accurate terrain mapping for navigation. | High-resolution mapping improves navigation accuracy, object detection, and obstacle avoidance, which are essential for safe and efficient driving. | High (2) |
| 3. Affordability of LiDAR/Radar street signs. | To be implemented widely across cities and road networks, the system must be cost-effective and scalable. | High (2) |
| 4. Reliability and user trust. | For AV adoption to increase, users must feel confident in the technology's performance under all driving conditions. | Critical (1) |

Safety and reliability were identified as critical because they are directly related to public acceptance and usability. Users and experts consistently emphasized that without dependability and reliability for safety features, autonomous driving cannot achieve full trust or widespread use and acceptance. Accurate terrain mapping ensures functionality with navigation and responsiveness to the driving environment, while affordability ensures the feasibility of integrating LiDAR and Radar technology into a national-scale infrastructure.

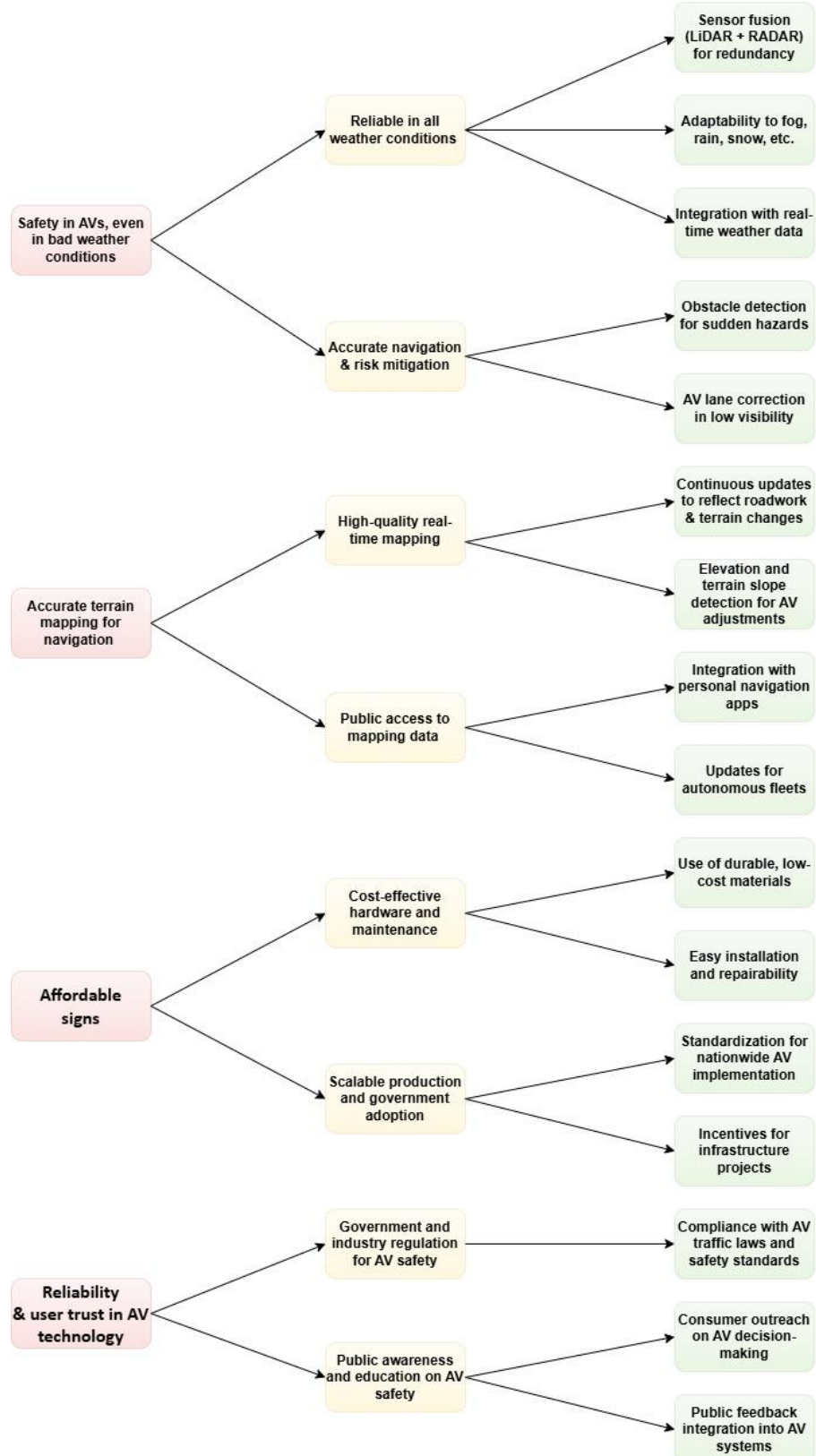


Figure 5. Tablature of tiered importance on the design of final prototype.

To narrow down what we would want our design to look like for testing, we created a decision matrix with multiple ideas that would solve the problem autonomous vehicles have in poor weather conditions. The final six ideas we came up with were the hollow sign, heating normal street signs, using satellite GPS, doppler radar, ultrasonic sonar, and vehicle-to-vehicle communication.

Table 2. Solution ideas and ranking

| Criteria | Weather Adaptability | Maintenance | Reliability | Power Requirements | Simplicity | Cost | Total (With Weights) |
|---|----------------------|-------------|-------------|--------------------|------------|------|----------------------|
| Weight | 30% | 10% | 20% | 15% | 10% | 15% | - |
| Hollow Sign | 5 | 5 | 4 | 5 | 5 | 5 | 4.80 |
| | 1.5 | 0.5 | 0.8 | 0.75 | 0.5 | 0.75 | |
| Heated Traditional Sign | 5 | 4 | 4 | 3 | 4 | 5 | 4.30 |
| | 1.5 | 0.4 | 0.8 | 0.45 | 0.4 | 0.75 | |
| Satellite GPS RTK | 3 | 3 | 4 | 3 | 2 | 2 | 2.95 |
| | 0.9 | 0.3 | 0.8 | 0.45 | 0.2 | 0.3 | |
| Doppler Radar | 5 | 3 | 5 | 3 | 4 | 2 | 3.95 |
| | 1.5 | 0.3 | 1 | 0.45 | 0.4 | 0.3 | |
| Ultrasonic Sonar | 3 | 3 | 3 | 4 | 4 | 4 | 3.40 |
| | 0.9 | 0.3 | 0.6 | 0.6 | 0.4 | 0.6 | |
| Vehicle-to-vehicle communication & phones | 5 | 5 | 4 | 4 | 2 | 3 | 4.05 |
| | 1.5 | 0.5 | 0.8 | 0.6 | 0.2 | 0.45 | |

After assessing how well we thought each idea would perform under the various criteria, we determined the hollow sign would be the best choice for our group to work on and test. We then needed to determine the critical function of our project, and create experimental questions

that would test if our project could solve the critical function. We determined our critical function was the vehicle needed to attain relative location using only LiDAR and Radar imaging off of the sign. And experimental questions we created for our testing phase were: how will poor weather conditions affect signal/data quality, how does speed affect the received signal from the sign, and how does distance affect the received signal from the sign.

From there we developed an experimental plan that would be able to answer the questions listed above, and test our critical function. We would utilize a fog machine, snow machine, and a makeshift rain machine that we would design to test the most common types of bad weather conditions a vehicle would normally drive through. In the actual experiments, we would first test the sensors looking through the simulated bad weather while being stationary so see how the sensors react under the best possible conditions. Then we would begin testing when the sensors were attached to a moving vehicle, gradually increasing the speed of the vehicle from ~10 mph, and up to normal street level speeds.

We then needed to figure out roughly how long it would take to accomplish all of these tasks. To do this we created a rough outline of all of the tasks that would need to be accomplished in the two semesters we were given to complete the project and estimated how long each task would take. It ended up being around 330 hours total to complete the entire project. Knowing that and all of the tasks we needed to complete, we created a Gantt Chart to schedule our entire project.

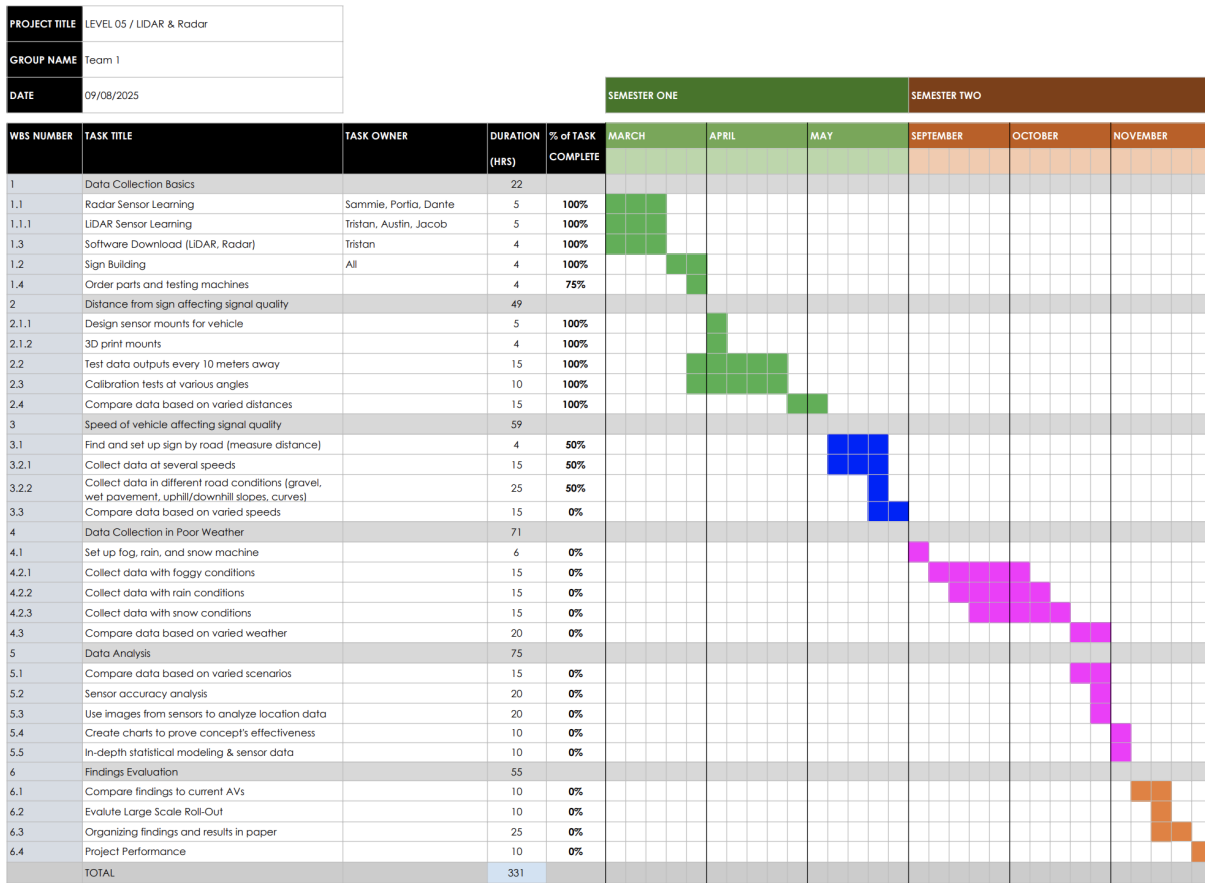


Figure 6. Gantt chart of responsibilities and dates of completion.

Finally, now knowing what we wanted to accomplish, and in what time constraints, we were able to figure out what materials we needed to purchase to accomplish our goals. Luckily, this project was inherited, and so the sign, and both the Radar and LiDAR sensors were donated to us, which greatly cut down on the potential cost of the project. We ended up buying a fog machine, a snow machine, liquid fog and snow for each machine to use, and finally a water hose to create our makeshift rain machine. This came out to \$240 of our budget, meaning we still have the majority of our budget available to us in case for a rainy day.

Design Specifications

The design specifications for the LiDAR/Radar street sign were developed to address the core issue of autonomous vehicle reliability in poor weather conditions. Drawing from the user needs, including safety, accuracy, reliability, and affordability, the specifications define measurable engineering targets that would ensure the system performs consistently in fog, rain, and snow while remaining practical for large-scale implementation.

Each metric was based on a combination of benchmarking existing AV technologies, technical expert feedback, and research on sensor performance under environmental interference. The selected values represent achievable yet important goals to guide design and testing decisions throughout the project.

Table 3. Design requirements and ranking

| Metric # | Specification | Goal Range | Comments |
|----------|--|---------------------------------|---|
| 1 | System reliability under low-visibility conditions | < 5 failures per 100,000 hours | Ensures dependable operation in fog, rain, and snow passenger safety |
| 2 | Sensor fusion accuracy (LiDAR + Radar) | > 95% object detection accuracy | Provides redundancy between sensing methods to strengthen reliability |
| 3 | Detection accuracy in bad weather | > 90% | Demonstrates consistent performance despite low visibility |
| 4 | Localization and mapping accuracy | < 0.5 m | Meets the lane-level precision required for AV navigation |
| 5 | Reaction time to obstacles | < 100 ms | Supports safe real-time perception and response |
| 6 | Mapping resolution | < 0.1 m per pixel | Provides detailed environmental data for navigation |
| 7 | Elevation and terrain slope detection accuracy | <0.2 m | Maintains accurate topographical information for route adjustments |
| 8 | Cost effective hardware and maintenance | < \$10,000 per year per sector | Keeps the system affordable and scalable for municipalities |
| 9 | Production scalability | > 10,000 units per year | Allows wide-scale manufacturing and deployment |
| 10 | Reliability and user trust in AV technology | > 80% user adoption rate | Supports public confidence in smart-infrastructure systems |

These metrics created the framework for evaluating all design decisions. For example, maintaining detection accuracy of 90 % or more in poor weather became a priority when comparing potential solutions. Similarly, the < 0.5 m mapping accuracy aligns with standard AV navigation tolerances, while the cost and scalability metrics ensure long-term usability for cities. These values define both the technical performance and practical boundaries of the project.

Brainstorming and Concept Development

To explore solutions, a tournament-style brainstorming method was used. Every member contributed ideas, then they were ranked and narrowed down collaboratively. This method made it easy to identify the best designs that balanced weather adaptability, reliability, simplicity, and cost.

Over twenty ideas were discussed, including heating traditional street signs and vehicle-to-vehicle communication systems. After evaluating each concept using a weighted decision matrix, several stood out:

1. Hollow Sign: A passive sign featuring internal cavities that reflect Radar signals in recognizable patterns.
 - a. Strengths: Does not require power, operates in all weather, and fits within existing infrastructure.
 - b. Weaknesses: Must balance size and shape to prevent excessive material use or visibility obstruction.
2. Heated Traditional Sign: Incorporates heating elements to keep surfaces free of ice and snow.
 - a. Strengths: Simple adaptation of current designs.
 - b. Weaknesses: Higher maintenance cost and energy consumption.
3. Satellite GPS Integration: Uses real time positioning to enhance navigation accuracy.
 - a. Strengths: Exceptional precision.
 - b. Weaknesses: Dependent on expensive infrastructure and continuous connectivity.
4. Doppler Radar Weather Detection: Uses radar to sense weather ahead of time.
 - a. Strengths: Improves awareness for AVs in changing conditions.
 - b. Weaknesses: Not easily implemented into fixed roadside systems.
5. Vehicle-to-Vehicle Communication Network: Shares environmental and sensor data between nearby vehicles.
 - a. Strengths: Expands awareness beyond onboard systems.
 - b. Weaknesses: Requires widespread adoption.

Each concept offered unique advantages and trade-offs. While some solutions were more technically complex or dependent on infrastructure, others were simpler and more scalable. The brainstorming process was essential for identifying how each approach addressed the core challenge of AV reliability in poor weather conditions. These insights formed the foundation for

the following design concept selection, where the team chose which ideas best met the performance and usability criteria.

Initial “back-of-the-envelope” engineering calculations on the preliminary designs

Even though our project had a predetermined design and prototype, we wanted to explore modifications to our current design and see if other technologies would be more applicable, given the goal of our project. For the preliminary “back-of-the-envelope calculations”, we explored different technologies such as ultrasonic and thermal sensors, as well as the design and limitations of the predetermined prototype.

Ultrasonic Sensors

The specific use of ultrasonic sensors would be for spatial awareness as well as for the potential use of specialized sign recognition along surface roads and highways. Pertinent data to the application includes the usefulness of the transceiver in cold and warm weather conditions as the temperature and relative density of the air increase or decrease, thus altering the speed of sound. Other conditions that may affect the data received and the subsequent usefulness of an application would include weather conditions, not limited to snow, sand, or rain, which may require testing and research, which is beyond the scope of any analysis done here.

For the purpose of analyzing the usefulness of ultrasonic sensing within AV sign and spatial recognition, several assumptions will be made in order to simplify calculations, but the resulting data will be sufficient to argue the application of ultrasonic sensors. It is assumed that the surrounding system will be isothermal as well as isobaric, as three separate systems will be analyzed at 1 atm with varying temperatures. When travelling in a vehicle, it can be assumed that the temperature of the surrounding air and the pressure will be nearly identical to allow the assumption. It is also assumed that the air surrounding the sensor is an ideal gas of homogeneous composition and is considered to be “dry” or without humidity and air vapor, which only improves the propagation of ultrasonic sound waves. In order for the sensors to be deemed successful in these situations, they must report data back in less than the human response time of 250 milliseconds. The temperatures at which the analysis will be made are 45 °C, 15 °C, and -15 °C in order to measure the effectiveness of a system in different temperature climates to ensure that data can be relayed quickly enough.

The equation that was used to measure distance by ultrasonic sound

$$X(m) = \frac{\left[C \left(\frac{m}{s} \right) * t(s) \right]}{2} \quad [1]$$

Equation 1: m – distance (meters) C – Speed of Sound (meters/ second) t – time (seconds)
The speed of sound must not be generalized in this particular application as factors such as the density of the fluid and related temperature do have an effect on the speed at which sound travels through the medium which in this case is air. Given the assumption of ideal gas properties, the bulk modulus is equivalent to the pressure of the gas.

$$C = \sqrt{(K/\varphi)} \quad [2]$$

Equation 2: K – Bulk Modulus (Pascals) φ – Density (kilogram/meter²)

Table 4: calculations for distance sensors are usable in differing temperatures

| Equation | | | | |
|------------------------|---------------------------------------|--------|--------|--------|
| Temperature (C) | - | 45 | 15 | -15 |
| Pressure (Kpa) | - | 101.3 | 101.3 | 101.3 |
| Density (Kg/m^3) | $\varrho = Pm / RT$ | 1.108 | 1.225 | 1.367 |
| Bulk Modulus (KPa) | K | 101.3 | 101.3 | 101.3 |
| Speed of Sound (m/s) | $C = \sqrt{K / \varrho}$ | 302.37 | 287.57 | 272.22 |
| Max Distance (m) | $X = (C * t) / 2$ (time = 0.250 s) | 37.80 | 35.95 | 34.03 |

Given the results from the analysis as seen above in Table 4 it is clear that with the sensors operating at temperatures ranging from 45 °C to -15 °C, which are extreme driving conditions, the maximum distance such a system could be used at is 34.03 meters with a 0.250-second response time. With current equipment, most ultrasonic sensors do not extend past 5 meters for automotive use; thus, the time required for the sound to return could be reduced beyond 0.250 seconds for a more responsive system and better decision-making on the vehicle's end. This analysis gives an explanation for the use of ultrasonic sensing in data collection for AVs while driving, although concerns for the use of ultrasonic sensing does include the effect of weather on the propagation and receiving of sound waves. Benefits of the use of sound waves in comparison to light or radar is that light sources and reflective materials do not affect the quality of reflected sound waves, but further research and potential testing must be done to compare the three modes of data collection. From this analysis it would be plausible to continue forward with

the testing and research of the use of ultrasonic sound to aid in the improvement of automated vehicle data collection.

Thermal Sensors

This analysis examines the feasibility of utilizing a thermal infrared (IR) sensor for autonomous vehicles (AV) sign recognition in adverse weather conditions. The purpose is to determine whether a thermal sensor can outperform a standard visible-light camera when fog, rain, or other weather conditions reduce visibility. The analysis focuses on how infrared radiation travels through fog and rain compared to visible light, evaluating how much signal is lost over distance. The thermal sensing concept will be considered effective if it maintains stronger signal clarity and contrast than a conventional optical camera under equivalent conditions.

For the assumptions, the sign was modeled as a blackbody emitter maintained at a constant temperature of 40 °C (313 K), ensuring it is thermally distinct from the ambient environment. Using Wien's displacement law, the dominant emission wavelength of the sign is approximated as

$$\lambda_{max} = \frac{b}{T} = \frac{2.94 * 10^{-3}}{313} = 9.4 \mu m \quad [3]$$

Equation 3: λ_{max} – Peak Emission Wavelength (meters), T – Absolute Temperature (Kelvin),
b – Constant of Proportionality (meter*Kelvin)

The target sign is assumed to be at a distance of 10 m, and attenuation due to fog and rain is modeled using Beer-Lambert's Law:

$$I(x) = I_0 e^{-\alpha x} \quad [4]$$

Equation 4: $I(x)$ – Transmitted Intensity ($\frac{W}{m^2}$) I_0 - Initial Intensity ($\frac{W}{m^2}$) α – Attenuation Coefficient (m^{-1}) x - distance (meters)

For fog, $\alpha_{IR} = 0.7 \text{ m}^{-1}$ and $\alpha_{visible} = 15 \text{ m}^{-1}$ yielding intensity ratios at 10 m of $I_{IR}(x) = 9.1 * 10^{-4} \frac{W}{m^2}$ and $I_{visible}(x) = 7.2 * 10^{-66} \frac{W}{m^2}$. For rain, $\alpha_{IR} = 0.002 \text{ m}^{-1}$ and $\alpha_{visible} = 0.005 \text{ m}^{-1}$, producing $I_{IR}(x) = 9.8 \frac{W}{m^2}$ and $I_{visible}(x) = 9.5 \frac{W}{m^2}$. These results indicate significantly reduced attenuation for infrared wavelengths under both fog and rain conditions.

These results demonstrate that infrared radiation experiences substantially lower attenuation in both fog and rain compared to visible light, confirming the potential of thermal sensors for sign recognition in harsh weather conditions. A sign heated to 40 °C and emitting predominantly at 9.4 μm would maintain detectable thermal contrast even when optical visibility is severely degraded. While further analysis should incorporate varying distances and ambient temperatures, the simplified model supports the plausibility of thermal sensors outperforming conventional cameras in low-visibility scenarios.

Thermal System for Snow-Free Street Signs

This concept analyzes a thermal system integrated into a street sign to prevent snow accumulation. Even though this analysis could be done in unison with the previous concept, this was completed with the assumption that the sign would maintain a surface temperature above 0 °C (32 °F) in typical winter conditions. This analysis aims to determine how much heat must be supplied to melt snow and offset heat losses.

This system is analyzed under steady-state conditions, assuming a surface temperature of 4 °C and an ambient air temperature of -10 °C. A moderate wind is considered, giving a convective heat transfer coefficient of 25 W/m² K. The sign is made of 5052-H38 aluminum (emissivity = 0.8) with a surface area of 0.5 m². Snowfall is modeled at a medium rate of 1.2 in/hr, corresponding to a snow depth rate of $8.5 \times 10^{-6} \text{ meters/sec}$.

The volumetric flow rate of snow is

$$V_{flow\ rate} = A \times V_{snow} = 0.5 \text{ m}^2 \times 8.5 \times 10^{-6} \frac{\text{m}}{\text{s}} = 4.25 \times 10^{-6} \frac{\text{m}^3}{\text{s}}$$

Assuming a snow density of $\rho = 200 \text{ kg/m}^3$, the mass flow rate becomes

$$m_{flow\ rate} = V \times \rho = 4.25 \times 10^{-6} \frac{\text{m}^3}{\text{s}} \times 200 \frac{\text{kg}}{\text{m}^3} = 8.5 \times 10^{-4} \frac{\text{kg}}{\text{s}}$$

To heat snow from -10 °C to 0 °C and then melt it:

$$Q_{warm} = m_{flow\ rate} c_{ice} \Delta T = 8.5 \times 10^{-4} \frac{\text{kg}}{\text{s}} \times 2100 \text{ J/kg} \cdot \text{K} \times 10 \text{ °C} = 18 \text{ W}$$

$$Q_{melt} = m_{flow\ rate} L_f = 8.5 \times 10^{-4} \frac{\text{kg}}{\text{s}} \times 334,000 \text{ J/kg} = 284 \text{ W}$$

$$Q_{\text{warm}} + Q_{\text{melt}} = 302 \text{ W}$$

Convective and radiative heat losses are then estimated as

$$Q_{\text{conv}} = h A (T_{\text{sign}} - T_{\infty}) = 25 \frac{\text{W}}{\text{m}^2 \text{K}} \times 0.5 \text{ m}^2 \times (277 \text{ K} - 263 \text{ K}) = 175 \text{ W}$$

$$Q_{\text{rad}} = \epsilon \sigma A (T_{\text{sign}}^4 - T_{\text{amb}}^4) = 0.8 \times 5.67 \times 10^{-8} \frac{\text{W}}{\text{m}^2 \text{K}^4} \times 0.5 \text{ m}^2 \times (277^4 \text{ K} - 263^4 \text{ K}) = 25 \text{ W}$$

The total heating power required is approximated as

$$P = 302 \text{ W} + 175 \text{ W} + 25 \text{ W} = 502 \text{ W}$$

Preliminary calculations show that a heating power of 502 Watts is required (varying with wind speed and snowfall rate) to keep a 0.5 m² sign surface above freezing in -10 °C ambient air. This power level is attainable from many existing power sources (grid or solar with battery). However, in extreme weather conditions, additional power or improved insulation may be necessary. The power required to melt a snow-covered sign increases as the temperature of ambient air decreases and the speed of the wind increases. Overall, the concept appears technically feasible for typical weather conditions.

Bolt Designing For Sign Prototype

To better improve the visibility of AVs (Autonomous Vehicles) in poor weather conditions, a sign should be placed to give a unique signal back to the AV. To make sure the signs are supported well, calculations for the bolts were conducted so that the sign would be supported properly. The bolt was assumed to have a diameter of 1/4 inch x 20 UNF bolt with a standard hexagonal nut and 1/4 N Steel plain washer attached. The bolt's length and spring rate were found so that the correct bolt could be applied in the sign application with a valid spring rate (k_b) so that the bolt would not get warped when compressing the joints together. The important characteristics when calculating the length include the distance the bolt will need to travel across for the different members. For the bolt k_b , the important factors are minor diameter area (A_t), threaded length (L_t), grip length (ℓ), and threaded and unthreaded portion in grip (ℓ_t and ℓ_d). The stresses in the bolts were also looked at to make sure that the shear and crushing stresses were found to make sure they were not impractical. For the stresses, it was assumed to have a design factor (n_d) of 1.5, and the bolt had an SAE standard of 5. From the calculations, it was determined that the bolts described are more than feasible to hold the sign above.

To analyze the system, a model was created to give a visual representation of the system (Figure 7), which helps to see each distance that the bolt has to travel through.

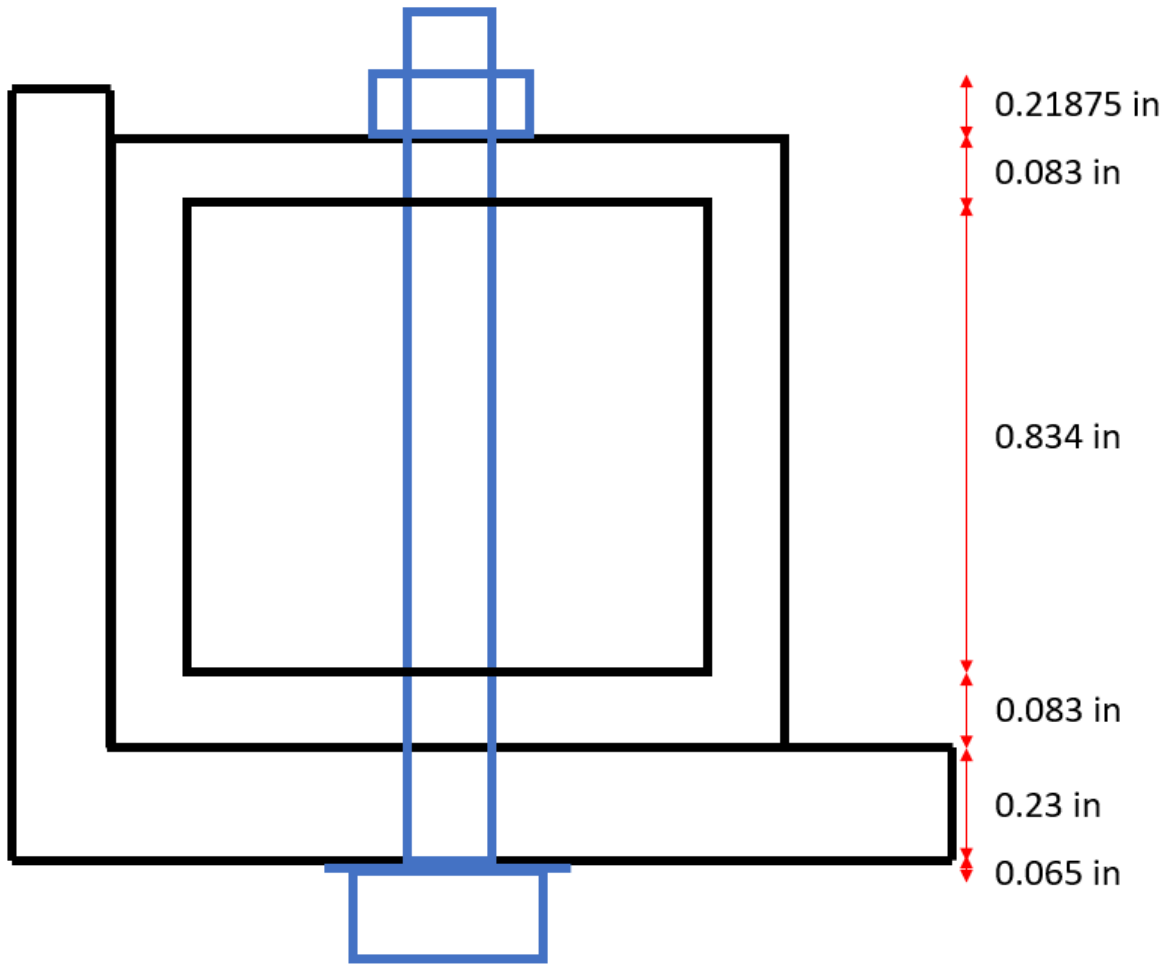


Figure 7. Model of Street Sign Bolt Configuration

The following analysis serves to analyze the LiDAR/Radar Street sign prototype in the case that it is struck by a moving vehicle. It will first determine the vehicle's speed required to break the legs of the sign. The failure mode solved for will be tensile bending stress at the critical point on the post. This will provide information on the integrity of the street sign. This failure is critical to the sign because it would cause the sign to fall over. The second analysis will consider the effect of colliding with the street sign. Here, the car's state will be predicted based on the speed at which it was traveling. This will give information on the safety of the driver under different conditions. Both analyses will consider a 2010 Honda CRV-EX (3500 lbs) colliding with the sign head-on. AAA has done an extensive study of these vehicles' crash properties that will be used to support the vehicle damage portion. This car represents the average size and age of cars in America [1]. A head-on collision would be likely if a car is driving off the road, and this analysis will be performed for simplicity. This assumes the car contacts both front legs of the sign at the same time. Also, a collision time of 0.05 seconds will be assumed which is

appropriate for a rigid collision such as a street sign. In reality, a higher-speed collision would have a slightly higher collision time because it would take longer for the vehicle to come to rest. These changes are assumed to be negligible.

Damage to sign:

$$F = \frac{m * \Delta v}{\Delta t} = \frac{3500 \text{ lbs} * v \text{ m/h}}{0.05 \text{ s}} * \frac{\frac{1 \text{ ft}}{s}}{\frac{0.681818 \text{ m}}{h}} = 102677 * v \text{ lbf}$$

Each pole will take on half of the force distributed by the car. If the contact point is 19 inches off the ground, the moment on the base of the pole, which is mounted to the ground, is

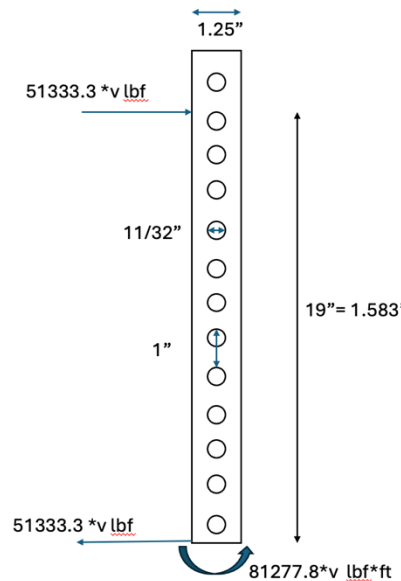


Figure 4: Free Body Diagram for sign post under stress

$$M = F * d$$

$$M = \frac{1}{2} * 102677 * v * \frac{19}{12} = 81278 * v \text{ lbf} * ft = 1.17 * 10^7 * v \text{ lb} * in$$

This is the critical point as it incurs the maximum moment and stress. The beam will break when the stress exceeds the maximum allowable stress for galvanized steel. It will break along the cross-section where the holes are cut out. The maximum allowable stress is 70000 psi [16]. Young's Modulus is 27.5E6 psi [6]. Stress calculations follow:

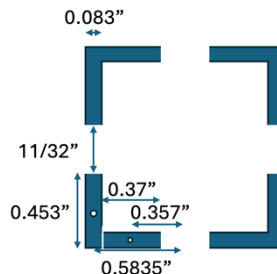


Figure 5: Cross sectional diagram of critical point at base of sign

$$I = \sum A_i r_i^2 = 4 * (0.083 * 0.453 * 0.5835^2 + 0.083 * 0.37 * 0.357^2) = 0.0528 \text{ in}^{-4}$$

$$\frac{r}{d} = \frac{\frac{11}{64}}{1.25 - 11/32} = 0.190$$

$$k_{conc} = 2.5 \quad \text{** see chart in appendix}$$

$$70000 = 2.5 * \frac{1.17 * 10^7 * v * 0.625}{27.5 * 10^6 * 0.0528} = V = 5560 \text{ mph}$$

The velocity required to cause the base of the street sign to fail in tensile stress due to bending would be 5560 miles per hour. This is not reasonable and supports the current street sign design. Assuming the maximum speed a car travels is 80 mph, this has a factor of safety of 69.5 which is sufficient to cover the assumptions made earlier regarding striking position and car specifications. This design is safe against bending tensile failure under all reasonable conditions. Lower velocities would deform the structure but not take it out completely.

The next analysis to be run includes the expected damages to a car at different speeds. This calculation is not as straightforward as the sign because it involves the crumbling of the front of the car which cannot be approximated as a homogeneous material. For this project, it will be appropriate to analyze a AAA crash test research paper and compare it with this design. Predictions will be made regarding the driver's safety under different conditions.

First, the similarities and differences will be noted between AAA's 2021 *Impact of Speeds on Drivers and Vehicles-Results from Crash Tests* and this street sign prototype crash analysis. This paper researches driver safety for a car traveling 64.4 km/h (40 mph), 80 km/h (50 mph), and 90 km/h (55.9 mph). Each car strikes a solid body head-on that extends across the driver's half of the car plus a few inches onto the driver's side [15]. The stopping time in these experiments aligns with the assumptions made in the previous calculations. The same kinetic energy transfer will occur at the same speed when struck by a solid object or by a street sign. The points of contact will be different between a solid wall and two posts. The failure of the car will depend on the geometry of its internal components and the collision front. The results can be approximated using the results from AAA's research because the same speeds will yield the same kinetic energy, producing similar damage. The accelerations can be analyzed to find the collision time in their experiments.

Table 5: Accelerations for three test cars at different speeds as they come to a stop from AAA's *Impact of Speeds on Drivers and Vehicles-Results from Crash Tests* [1]

| | Test 1 | Test 2 | Test 3 |
|------------------------------------|--------|--------|--------|
| Target velocity (km/h) | 64.4 | 80.5 | 90.0 |
| Actual impact velocity (km/h) | 64.4 | 80.5 | 89.8 |
| Peak longitudinal acceleration (g) | -36.9 | -46.8 | -55.5 |
| Delta-V (km/h) | 72.9 | 87.7 | 99.0 |

$$a = \frac{\Delta v}{\Delta t}$$

For test 1: $36.9 * 9.81 (\frac{m}{s^2}) = \frac{64400(\frac{m}{s})}{3600} / \Delta t(s)$; $\Delta t = 0.049$ seconds

For test 2: $46.8 * 9.81 (\frac{m}{s^2}) = \frac{80500/3600(\frac{m}{s})}{\Delta t(s)}$; $\Delta t = 0.048$ seconds

For test 3: $55.5 * 9.81 (\frac{m}{s^2}) = \frac{90000/3600(\frac{m}{s})}{\Delta t(s)}$; $\Delta t = 0.046$ seconds

The collision time for each of these experiments is very close to the assumed time of 0.05 seconds. These signs will be assumed to exert similar damages to vehicles because the accelerations and energy transfer are similar. As the velocity, the kinetic energy transfer increases exponentially with experiment 2 involving 56% more energy and experiment 3 involving 95% more energy than experiment 1 [1].

Table 6: Results from three crash tests from AAA's *Impact of Speeds on Drivers and Vehicles-Results from Crash Tests* [1]

| | Test 1 40 mi/h (64.4 km/h) | Test 2 50 mi/h (80 km/h) | Test 3 55.9 mi/h (90 km/h) |
|------------------------------------|----------------------------------|--------------------------------|----------------------------------|
| Overall evaluation | G | P | P |
| Structure | G | G | P |
| Restraints & Kinematics | G | A | P |
| Driver injury measures | | | |
| Head/neck | G | P | P |
| Chest | G | A | P |
| Left leg | G | G | A |
| Right leg | G | P | P |

Note: The overall rating and each measurement for a vehicle's crashworthiness can be good (G; the highest rating), acceptable (A), marginal (M), or poor (P; the lowest rating).

These results show it is most dangerous for a driver to strike a sign at speeds at or above 50 miles per hour. The same can be assumed to hold for the sign prototypes. These calculations show the concerns in a collision accident should be focused on driver safety. The sign will stay standing up to vehicle speeds of 5560 mph. This sign has an extra post to support the weight compared to a traditional speed limit sign with one post. Therefore, the force exerted on the car is greater because acceleration is increased. This puts the driver at higher risk.

Radar Analysis with the Hollow Sign

The goal of this analysis is to determine the detectability of the hollow sign by the radar and to identify potential indications of a unique signal produced by the hollow cavity. First, the radar cross-section of the plate is calculated to see how much of the signal will be reflected to the radar. This is used for the detectability of the sign, taking into consideration the wavelength at which the radar operates and the size of the sign. Using the detectability of the sign, the max range that the radar could operate at is calculated. This considers the potential losses that could occur during harsh conditions as well as the operating specifications of the radar. The analysis also includes the effect of the hollow cavity and the delayed signal that will be created due to the front and back plates of the sign. This will give us insight into a part of the unique signature produced by the sign.

| | |
|---------------------|--|
| Radar Specification | 79 GHz Antenna Gain 18 dB Power Transmitted 13 dBm Power Received -90 dBm |
| Sign Dimensions | Outer Face 24"x 24" Inner Face 16" x 16" Depth 8" |
| Assumptions | - Radar normal to sign - No signal scattering - Estimated signal loss value - Sign approximated as flat plate |

Frequency to wavelength conversion for 79 GHz; where ‘f’ (Hz) is frequency and ‘c’ is the speed of light (m/s)

[5]

$$\lambda = \frac{c}{f} = \frac{3 \times 10^8}{79 \times 10^9} = 0.0038 \text{ m}$$

Radar Cross Section of Equivalent Flat Plate [1] where A_{eff} is the outer reflective face of the sign. Using the conversion for the dimension of 1 inch = 0.0254 meters.

[6]

$$\sigma_{max} = \frac{4\pi A_{eff}^2}{\lambda^2} = \frac{4\pi(0.6096^2 - 0.4064^2)^2}{0.0038^2} = 37092 \text{ m}^2$$

This value is extremely high, this could be caused by variables that are not accounted for in this equation. Some assumptions relating to this are that it is a perfectly conducting surface, has no losses, is normal to the radar, has no scattering of the signal and has no distance limitations. Even though the value is extreme, it shows us that the higher frequency radar will produce a higher radar cross-section.

Radar Equation for max effective distance [13] where ‘G’ is the antenna gain, $'P_t'$ (W) is power transmitted, $'P_{r,min}'$ is minimum power received, ‘R’ is the distance, and ‘L’ is the potential losses. Using the conversion of decibels to linear

$$G = 18 \text{ dB} = 10^{\frac{18}{10}} = 63.1; P_t = 13 \text{ dBm} = \frac{10^{\frac{13}{10}}}{1000} = 0.02 \text{ W}$$

$$P_{r,min} = -90 \text{ dBm} = \frac{10^{\frac{-90}{10}}}{1000} = 10^{-12} \text{ W}; L = 12 \text{ dB} = 10^{\frac{12}{10}} = 16$$

[7]

$$R_{max} = \left(\frac{P_t G^2 \lambda^2 \sigma}{(4\pi)^3 P_{r,min} L} \right)^{\frac{1}{4}} = \left(\frac{0.02 \times 63.1^2 \times 0.0038^2 \times 37092}{(4\pi)^3 \times 10^{-12} \times 16} \right)^{\frac{1}{4}}$$

$$R_{max} = 191.4 \text{ m}$$

This value shows that the sign will be detectable at long distance away from the radar given the dimensions of the sign. This formula assumes that there will be one antenna that transmits and receives the signal which is common in autonomous vehicles. Lastly, an assumed value of a 12 dB loss that translates to a 50% loss of range due to harsh conditions [8].

Range or distance measurements [11]

[8]

$$t = \frac{2d}{c}$$

Time for the radar signal to travel to the sign and back at 100 meters

$$t = \frac{2 * 100}{3 * 10^8} = 667 * 10^{-9} \text{ sec}$$

Time delay of the second signal due to the hollow cavity (depth of 8")

$$t = \frac{2 * 0.2032}{3 * 10^8} = 1.35 * 10^{-9} \text{ sec}$$

This will show a signal of similar magnitude, but at a slight delay from the first one providing a part of the unique signature that the sign produces.

The radar cross-section that the sign will return is extreme compared to real world data even with the high-resolution radar and this is caused by losses that are not considered in the formula. The max range of the radar was calculated with consideration of the high cross-section and harsh conditions that will be tested by assuming a 50% loss of range. This showed that the sign will be detectable at ranges that are necessary for autonomous vehicles.

Table 7. Solution ideas and ranking

| Criteria | Weather Adaptability | Maintenance | Reliability | Power Requirements | Simplicity | Cost | Total (With Weights) |
|---|----------------------|-------------|-------------|--------------------|------------|------|----------------------|
| Weight | 30% | 10% | 20% | 15% | 10% | 15% | - |
| Hollow Sign | 5 | 5 | 4 | 5 | 5 | 5 | 4.80 |
| | 1.5 | 0.5 | 0.8 | 0.75 | 0.5 | 0.75 | |
| Heated Traditional Sign | 5 | 4 | 4 | 3 | 4 | 5 | 4.30 |
| | 1.5 | 0.4 | 0.8 | 0.45 | 0.4 | 0.75 | |
| Satellite GPS RTK | 3 | 3 | 4 | 3 | 2 | 2 | 2.95 |
| | 0.9 | 0.3 | 0.8 | 0.45 | 0.2 | 0.3 | |
| Doppler Radar | 5 | 3 | 5 | 3 | 4 | 2 | 3.95 |
| | 1.5 | 0.3 | 1 | 0.45 | 0.4 | 0.3 | |
| Ultrasonic Sonar | 3 | 3 | 3 | 4 | 4 | 4 | 3.40 |
| | 0.9 | 0.3 | 0.6 | 0.6 | 0.4 | 0.6 | |
| Vehicle-to-vehicle communication & phones | 5 | 5 | 4 | 4 | 2 | 3 | 4.05 |
| | 1.5 | 0.5 | 0.8 | 0.6 | 0.2 | 0.45 | |

Previously listed customer requirements were used in the decision matrix in table 7. The hollow design concept scored greater than nearly all other solutions in every category and thus it was selected for further proof of concept testing. Ultimately the total weight of the hollow sign stood atop the matrix as the solution that would be pursued which entailed the use of Radar and Lidar sensors to produce signatures usable by automated vehicles in poor weather conditions which was the primary goal.

Proof of Concept Testing

With an initial concept in mind, testing must be done to ensure that the provided solution is in fact attainable as well as repeatable. To re-emphasize the critical function, it is once again to attain relative location using only LiDAR and Radar images. It is crucial that a car can use these signs alone to locate itself when the road conditions cannot be used. The acceptable error for location is plus or minus 6 inches in both coordinate directions. The car's location must be within this criteria at any one point. It may take several scans as the car approaches the sign to use in its analysis and the test procedure is as follows:

- **Given the operation frequencies of Radar and LiDAR at 79 GHz and 30 Hz respectively, how will poor weather conditions affect signal/data quality?**
 - The team will simulate poor weather conditions.
 - A fog machine will be used to simulate the received signal/data quality during fog.
 - A rain machine designed by the team will be used to simulate the signal/data quality received during rain.
 - A snow machine will be used to simulate signal/data quality during snow storms.
- **How does speed affect the received signal from the sign?**
 - The LiDAR and Radar will be mounted to different surfaces traveling at different speeds.
 - The sensors will measure signals from walking speed.
 - The sensors will measure signals at a moderate speed (bike, skateboard).
 - The sensors will measure signals at an accelerated speed (Electric skateboard, car).
- **How does distance affect the signal quality from the sign?**
 - Will the LiDAR and Radar operate and collect reliable data at different distances from the sign?
 - The sign will be placed at incremental distances of +5 ft from the sensors starting at 10ft.
- **How does the incidence angle of the Radar affect the signal returned?**
 - Will a similar signal be received when using the Radar facing the sign face at increasingly large angles?
 - The Radar will be placed at 30 degrees and tests repeated every 15 degrees until -30 degrees.

Proof of concept testing was completed in April of 2025 and results compiled following the completion of those experiments. Alongside the testing using Radar at the ASU Chandler Innovation Center, Ansys simulations software was used to indicate the expected shape and magnitude of the image generated by a received Radar signal as shown in figure 3.

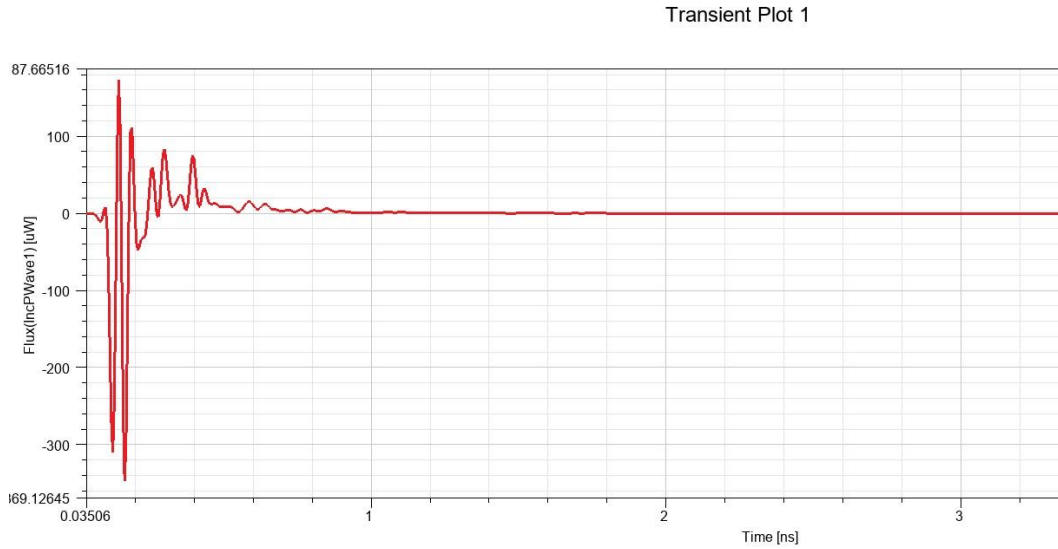


Figure 8. Flux versus time graph of a radar signal

As seen in Figure 8, the returned signal with the presented design will result in two distinct peaks, one of greater and the second of a lesser magnitude to indicate that the signal is unique from any surrounding structures or street signs. Another simulation was created to simulate the e-field or a visual representation of the strength of the returned signal in V/m in order to ensure that the final design would most efficiently fulfill the requirements laid out previously. In Figure 9 it can be seen the areas of greatest return and strongest Radar signal would be at the corners of the orifice as well as at the center. This realization aided in the modification of the sign face by adding a metal sheet in the center to bifurcate the orifice in order to improve the dual peak signal by placing the metal where the signal would be seen in greater magnitude.

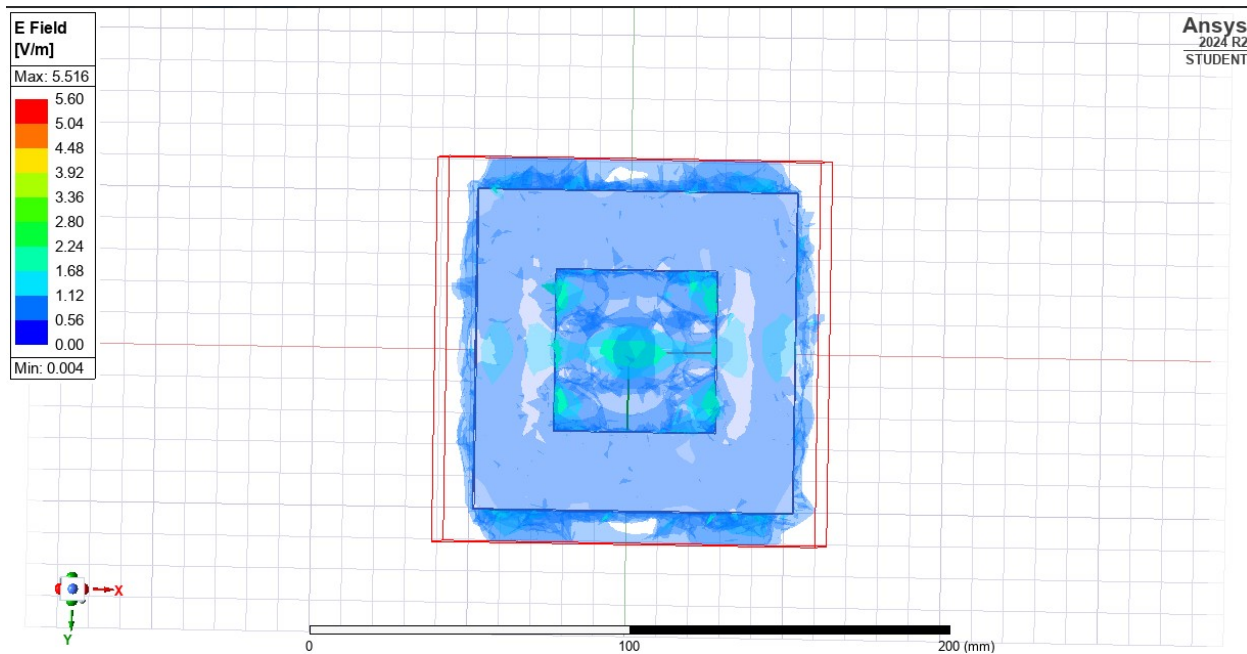


Figure 9. E-field analysis of the sign to represent the greatest areas of Radar return.

Results from the distance, speed, and angle testing confirm the simulation results with a return of two peaks, the first being of greater magnitude and the second of lesser. The trend as seen in the data follows this hypothesis as the magnitude of the first peak is relatively greater than the second. Figure 10 is a graphical representation across all distances and the relationship between the magnitudes of the peaks.

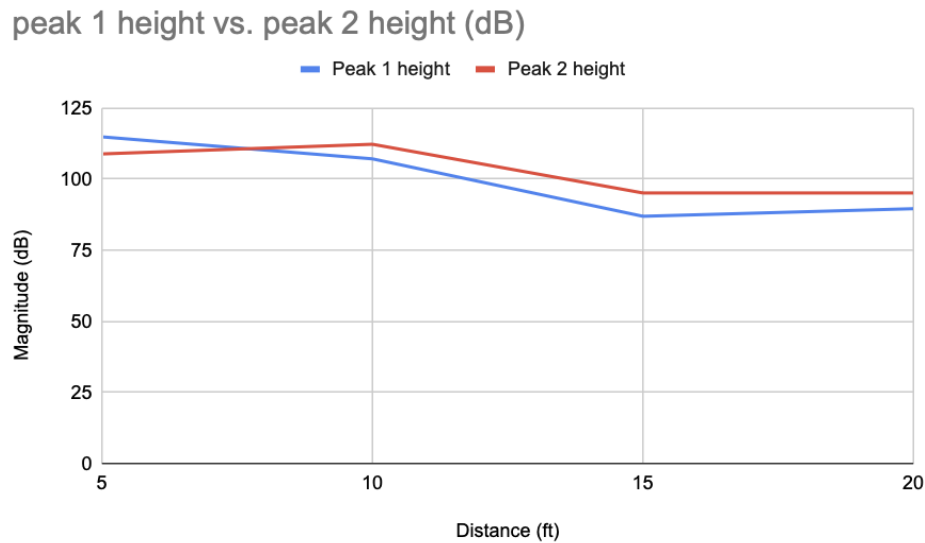


Figure 10. Relationship between first and second peak of Radar return.

The following test sequence was done at different angles from 30 to -30 degrees in 15 degree increments. Similar results were obtained to the previous figure and show proof of concept that the incident angle does not prevent or degrade the return signal.

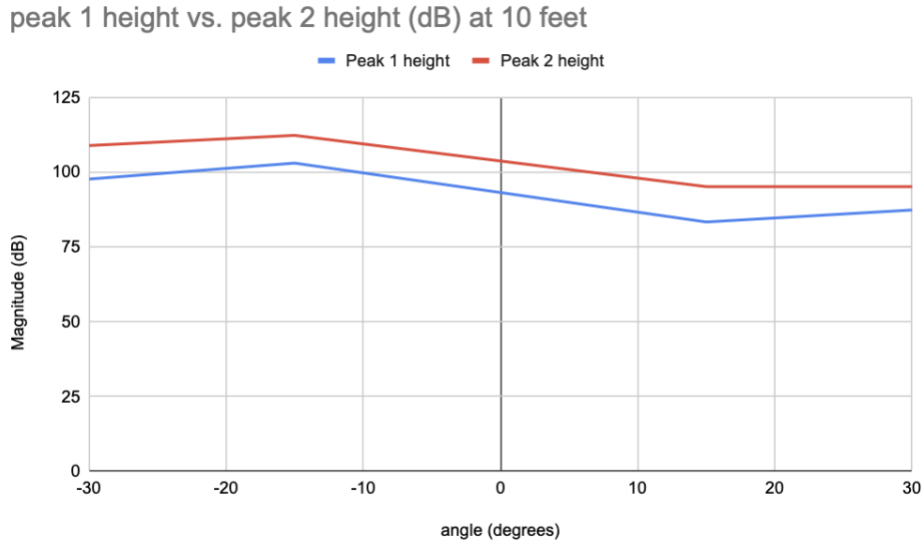


Figure 11. Graph of first and second peak in relation to incident angle.

These results in conjunction with the analysis within Ansys heavily influenced the final design and the adjustments made to the initial prototype. The orifice was ultimately bifurcated with a steel sheet thus providing a surface where the Radar return would be the greatest and making the dual peaks more pronounced. Initial testing with the first prototype showed that the results could be muddled and the magnitude of the peaks were similar to that of the surrounding noise. The simulation results only stood to reaffirm the initial hypothesis. Testing with the plate clamped to the face of the sign proved to be an improvement in the data and resulting graphs. It was decided that the change would then become permanent by welding the plate to the face of the sign thus resulting in the final prototype.

Final Design Details

The design for this project was initiated with a working prototype with a square hole.

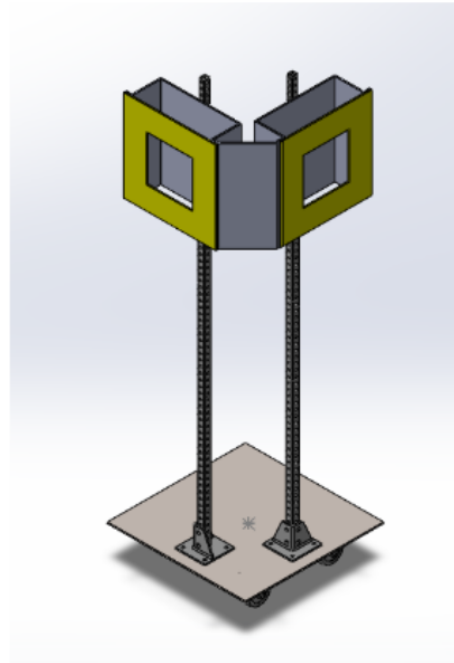


Figure 12. Initial sign prototype with square face

The final design was decided to be a bisected square hole because it provided consistent data in standard conditions, which acts as the control group. The sign front was permanently implemented by welding an additional plate to the face of the provided sign.

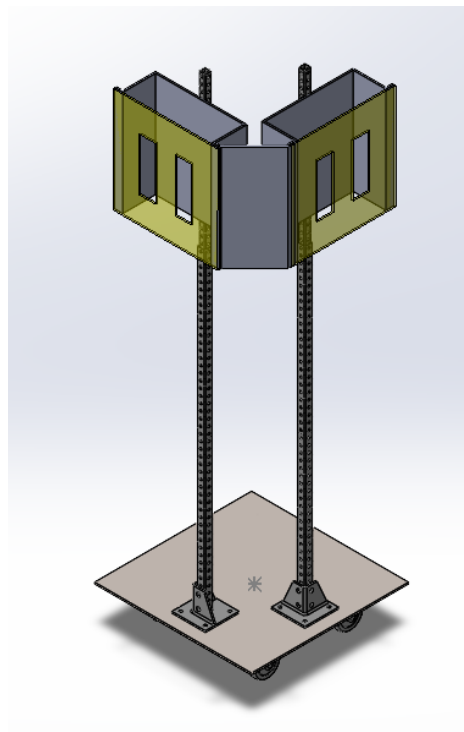


Figure 13. Modified sign face with bisected face CAD model



Figure 14. Modified sign face with bisected face prototype

For testing radar and lidar capabilities in poor weather conditions, additional materials and assemblies are required. The following Bill of Materials outlines parts needed.

Table 8. Bill of Materials for sign build and testing

| Hollow Sign | | | | |
|--------------|-----------|------------|-------------|--------------|
| Item | Quantity | Unit Price | Total Price | Manufacturer |
| Sign | 0 | \$0.00 | \$0.00 | Donated |
| LiDAR | 0 | \$0.00 | \$0.00 | Donated |
| Radar | 0 | \$0.00 | \$0.00 | Donated |
| Fog Machine | 1 | \$50.00 | \$50.00 | Amazon |
| Snow Machine | 1 | \$80.00 | \$80.00 | Amazon |
| Fake Snow | 3 Gallons | \$30.00 | \$90.00 | Amazon |
| Water Hose | 1 | \$20.00 | \$20.00 | Amazon |
| PVC Pipe | 10 ft | \$7.00 | \$7.00 | Home Depot |

The snow and fog machine were functional out of the box, but the rain simulator needed to be assembled.

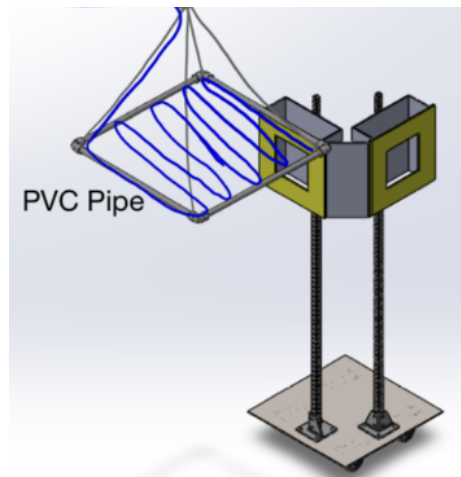


Figure 15. PVC square and hose routing to produce falling rain droplets.

The radar board also needed a mount so it could be held still for consistent scans. It allowed for rotation about the center post for dynamic scans while driving past the sign. The head tilt can be moved for different sign heights.

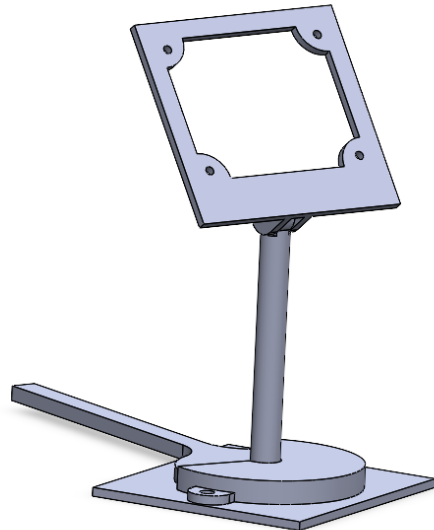


Figure 16. Radar mount CAD file



Figure 17. Radar mount prototype

These parts and assemblies create the foundation for a series of tests aimed to prove radar's superiority to LiDAR in poor weather conditions. The tests will be completed as follows: standard conditions, fog, snow, rain, in motion. It will be proved if weather conditions do not affect the radar's readings in situations when LiDAR fails. This would support the idea that radar will collect data from these signs when LiDAR can't. The next iteration of testing includes proving the sign geometry's effectiveness. It will be proved if a radar board can be located relative to a sign using several readings. It should differentiate the reading of a hollow sign from other objects that a car may drive past. Additional analysis will investigate how a moving radar board (like a car driving by) would impact data. These cumulative results and analysis have the potential to help locate vehicles in situations where current technologies fail.

Experimental Design

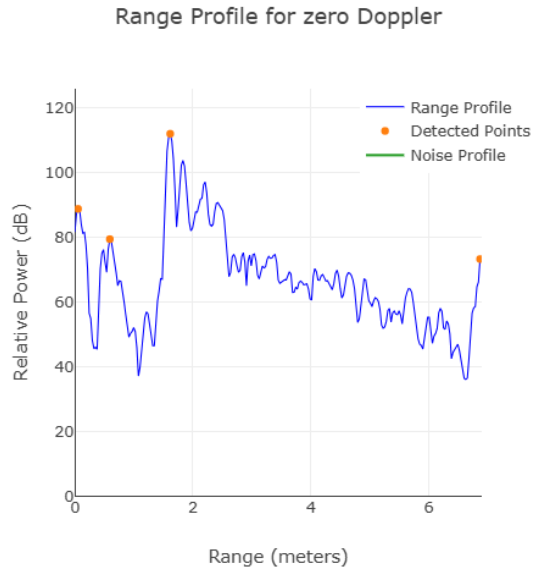


Figure 18. Radar signature at 5 feet straight on in good weather

This first experiment is structured to demonstrate that a hollow sign produces a consistent and repeatable radar signature, and to quantify how performance changes with varying viewing angles and adverse weather conditions. A dry, head-on configuration serves as the control baseline. Then variations in distance are introduced (10, 15, 20 feet), along with angle (-30, -15, 0, 15, 30) and weather (dry, fog, snow, rain) to evaluate robustness relative to that baseline. The negative angles are taken in a counterclockwise direction from the head-on angle, and the positive angles are taken in a clockwise direction.

Each condition is replicated with at least five trials to support confidence intervals and basic hypothesis tests. Sensor configurations and mounting geometry are held constant, and distance and angle are independently varied. Processing parameters are held constant across all runs, ensuring that radar features, such as peak locations and magnitudes, are presented comparably. LiDAR is recorded as a comparison to illustrate observability loss in fog and snow. Radar remains the primary focus.

This sign seeks to improve the accuracy of position measurements for autonomous vehicles in poor weather conditions. In order to improve these measurements, a unique radar signature is required so that software may differentiate a sign from other objects on the side of the road. After a literature review of radar techniques and theory, the hollow sign geometry was chosen. It should relay the relative position of the car to the sign. The focus of our project is just producing a unique signal that is still legible in a variety of bad weather conditions.

The control data was obtained in good weather straight on at 5 feet, 10 feet, 15 feet, and 20 feet from the radar sensor. Three trials were run at each distance. Statistical analysis was conducted to find confidence intervals for properties of the radar images. These include peak

magnitudes and distances of critical points [3]. We also experimented with the shape of the hole of the sign and found the double slit pictured below produced the most consistent results. We ran three tests at each distance to prove we can get consistent results, along with retesting the baseline before the weather tests to further prove the signal we are getting back is definitely from our sign, and it was consistent. The “0-degree” angle is used in angle testing to determine how the signature reacts at different incoming angles.



Figure 19. Test setup for angle testing at 30 degrees

Angle Variations

The angle was measured in reference to the 0-degree angle, with angles being taken at -30 degrees, -15 degrees, 15 degrees, and 30-degree angles. The experiments were run at 10 feet and 20 feet, with 3 trials per set. Filling in the control group at 10 and 20 feet for 0-degree angles, 30 images in total will be considered to find the effect of angle on radar scans. Statistical analysis will find confidence intervals for graph parameters as a function of angle.

Weather

To begin fog testing, a box is modified with a hole for the radar and a separate hole to allow the fog machine to fog up the box in a well-contained area, as seen in Figure 20. After 30 seconds of running the fog machine, the flaps of the box are opened, and the fog begins to dissipate from the box. Data is recorded during this process to ensure equal and similar results for the peaks as seen in the stagnant test results. Once again, testing the sign at different distances of 10 and 15 feet.



Figure 20. Test setup for fog testing using a box for containment

A snow machine is then placed on a cart propped up to shoot the snow particles in the direction of the sign in front of the radar to begin recording data to see if snow flying in front of the sign or snow buildup on the sign has any effect on the unique signature of the sign at varying distances of 10, 15, and 20 feet. Several sets of data points are taken over 15 seconds to ensure consistency in results during testing, and that the unique signature of the sign remains consistent throughout the testing phase.

A homemade rain machine consisting of a square PVC pipe with a hose wrapped in a snaking formation is zip-tied together and hung from an elevated area above the sign. Several holes are punctured through the hose to mimic the flow of rainwater, with one end of the hose being plugged up to help with pressure loss. Similar to the other tests, the sign readings are taken at several distances consisting of 10, 15, and 20 feet over a 15-second interval to ensure that the readings of the sign remain consistent and precise when compared to the other weather conditions (ie, snow, fog, dry). Having several data points will come in handy when calculating the percent error and standard deviations between the different sets of data points.

Sensor Settings

The tests were run with a Texas Instruments AWR1642BOOST radar, and an Intel RealSense LiDAR L515 was used in the following procedures [17]. The platform details were used to select the model of radar being used; in this case, we are using a WR16 model. The framerate should be dropped to 3 fps as faster rates limit the number of plots and measurement data that can be captured from the device. The range resolution should be set to 0.043 m, as this should be the minimum amount of separation expected between the detected objects in the point cloud. The maximum unambiguous range should be set to 6.66 m (21.85039 feet) to allow for a

little bit of excess range of our 20-foot testing distance. The maximum radial velocity should be set to 0.69 m/s, as the object is a stagnant sign; it is fine to use a smaller value here. Radial velocity resolution should be set to 0.05 m/s, as this is the lowest dependent parameter in this configuration and gets constrained by all the preceding parameters. The last parameter sets the desired cross-section to 3 sq. m, as this particle radar senses a motorcycle at 3.2 sq. m, which means it should have no problem sensing the sign. The LiDAR and radar were mounted to ensure consistent height and angle towards the sign [3].

Results

This results section documents how the prototype hollow sign performs relative to our engineering objectives and how that performance changes with view angle and adverse weather. We focus on radar observability and stability, comparing detected peak locations to true distance and tracking variability of peak magnitude. LiDAR was included as a comparison to check where optical returns degrade (fog, rain, snow).

For each image, two key radar peaks were identified: Peak 1 and Peak 2, and their corresponding magnitude (dB height) and location (distance reading) Table 9. Confidence intervals were calculated to estimate the true mean values of radar peak locations (in feet) and magnitudes (in decibels) under controlled conditions Table 9. The following describes each parameter as a function of distance under standard conditions for 95 % confidence.

$$Loc_{P1} = (0.97D + 0.08) \pm 0.41$$

$$Loc_{P2} = (0.98D + 0.74) \pm 0.49$$

$$Mag_{P1} = (-1.6D + 122.4) \pm 6.3$$

$$Mag_{P2} = (-0.9D + 117.6) \pm 8.2$$

Where D and Loc are in feet and Mag is in dB, respectively.

The radar measurements showed that the detected peak locations were closely aligned with the true target distances, indicating strong accuracy and consistency in distance detection. The narrow confidence intervals demonstrate that positional readings are both stable and repeatable, confirming the system's reliability under controlled conditions. In contrast, the magnitude data displayed greater variability, reflecting how signal strength naturally fluctuates with distance and environmental factors such as scattering and surface reflections. This variation is due to the way energy disperses and attenuates over range.

Standard deviations and error were also considered. The standard deviations for the control group show high precision in position and moderate variability in signal strength. For peak locations, standard deviations ranged from about 0.14 to 0.34 feet, indicating tightly clustered readings and strong repeatability. For peak magnitudes, standard deviations were larger, between about 2.0 and 6.3 dB, reflecting normal fluctuations in radar signal intensity due to environmental noise and scattering. These values correspond to distance percent errors of roughly 1 to 5 percent, confirming that measured target positions closely matched true distances.

Overall, the analysis confirms that the radar provides precise distance measurements and predictable signal behavior, forming a dependable baseline for evaluating how angular offsets and weather conditions may influence performance in later tests.

Angle Testing (Dry)

Angle performance was evaluated at fixed distances (10 and 20 feet) for angles -30°, -15°, 0°, 15°, 30° referenced to the sign's surface. Sensor configurations, mounting geometry, and processing methods matched the control group. Results are reported as condition means and are interpreted relative to the 0° baseline at each distance.

Results at 10 feet

At 0°, mean magnitudes were 107.1 dB (Peak 1) and 112.3 dB (Peak 2). Moving off-axis reduced return strength in a graded way: moderate angles ($\pm 15^\circ$) produced noticeably smaller peaks, and larger angles ($\pm 30^\circ$) produced the largest decreases. The response was asymmetric between positive and negative angles, consistent with the hollow cavity. Peak 2, in particular, weakened more on the 15° side than on the -15° side. Across angles, peak locations continued to track the true distance within the bounds established in the control group, indicating that angle primarily influences signal strength rather than range estimation.

At 10 ft, Peak 1 magnitude decreases from the 0° control by about 9-21 dB as the angle moves to $\pm 15^\circ$ and $\pm 30^\circ$. Peak 2 decreases by about 9-29 dB. The mean absolute distance error is 0.49-0.82 feet (4.9% - 8.2%) for Peak 1 and 0.17-0.61 feet (1.7% - 6.1%) for Peak 2.

Table 9. Angle Results at 10 feet (Dry)

Means \pm 95% CI; Deltas are relative to the 0° control at 10 feet (Peak 1 = 107.1 dB, Peak 2 = 112.3 dB). Location error = measured distance - true distance. dB to 1 decimal; feet to 2 decimals.

| Angle (°) | Peak 1 Mean \pm CI (dB) | Δ vs 0° P1 (dB) | Peak 2 Mean \pm CI (dB) | Δ vs 0° P2 (dB) | Loc P1 Mean Error (ft) | Loc P2 Mean Error (ft) |
|-----------|---------------------------|------------------------|---------------------------|------------------------|-------------------------|-------------------------|
| -30 | 93.0 \pm 2.48 | -14.1 | 97.7 \pm 1.43 | -14.6 | 0.60 | 0.28 |
| -15 | 91.7 \pm 1.43 | -15.4 | 103.0 \pm 2.48 | -9.3 | 0.82 | 0.17 |
| 15 | 98.0 \pm 2.48 | -9.1 | 83.3 \pm 1.43 | -29.0 | 0.71 | 0.61 |
| 30 | 86.7 \pm 1.43 | -20.5 | 87.3 \pm 1.43 | -25.0 | 0.49 | 0.50 |

Results at 20 feet

At 0°, mean magnitudes were 89.6 dB (Peak 1) and 95.1 dB (Peak 2). Angular reductions were the same or larger than at 10 ft, with $\pm 30^\circ$ again resulting in the largest decreases. Peak locations remained consistent with true distance, but the smaller magnitude margins at larger angles reduced detectability.

At 20 ft, Peak 1 decreases by 6-17 dB and Peak 2 by 7-15 dB across the same angles. Despite these differences, location accuracy remains stable. Peak 1 error is 0.32-0.54 feet (1.6% - 2.7%), and Peak 2 is 0.34 feet (1.7%) across all angles.

Table 10. Angle Results at 20 feet (Dry)

Means \pm 95% CI; Deltas are relative to the 0° control at 20 feet (Peak 1 = 89.6 dB, Peak 2 = 95.1 dB). Location error = measured distance - true distance. dB to 1 decimal; feet to 2 decimals.

| Angle (°) | Peak 1 Mean \pm CI (dB) | Δ vs 0° P1 (dB) | Peak 2 Mean \pm CI (dB) | Δ vs 0° P2 (dB) | Loc P1 Mean Error (ft) | Loc P2 Mean Error (ft) |
|-----------|---------------------------------|---------------------------|---------------------------------|---------------------------|-------------------------------|-------------------------------|
| -30 | 83.0 \pm 0.00 | -6.6 | 83.5 \pm 1.24 | -11.6 | 0.32 | 0.34 |
| -15 | 81.0 \pm 0.00 | -8.6 | 88.3 \pm 1.43 | -6.8 | 0.54 | 0.34 |
| 15 | 74.3 \pm 2.87 | -15.3 | 80.0 \pm 0.00 | -15.1 | 0.54 | 0.34 |
| 30 | 72.7 \pm 1.43 | -16.9 | 84.0 \pm 0.00 | -11.1 | 0.54 | 0.34 |

Angle mainly reduces return strength (most at $\pm 30^\circ$), while distance accuracy remains within the control tolerance at both 10 ft and 20 ft. This supports that angle affects detectability more than range estimation.

Modeling and Interpretation

Magnitude as a function of angle is represented well by the change in angle, showing a consistent decrease from 0° with stronger curvature at 20 ft. Within the tested range, location error did not exhibit a meaningful dependence on angle, supporting peak position as the primary metric and magnitude as a secondary. A practical operating region is $\pm 15^\circ$, which maintains stronger and more balanced signals at both distances. $\pm 30^\circ$ remains usable but with reduced detection margin, particularly at 20 feet.

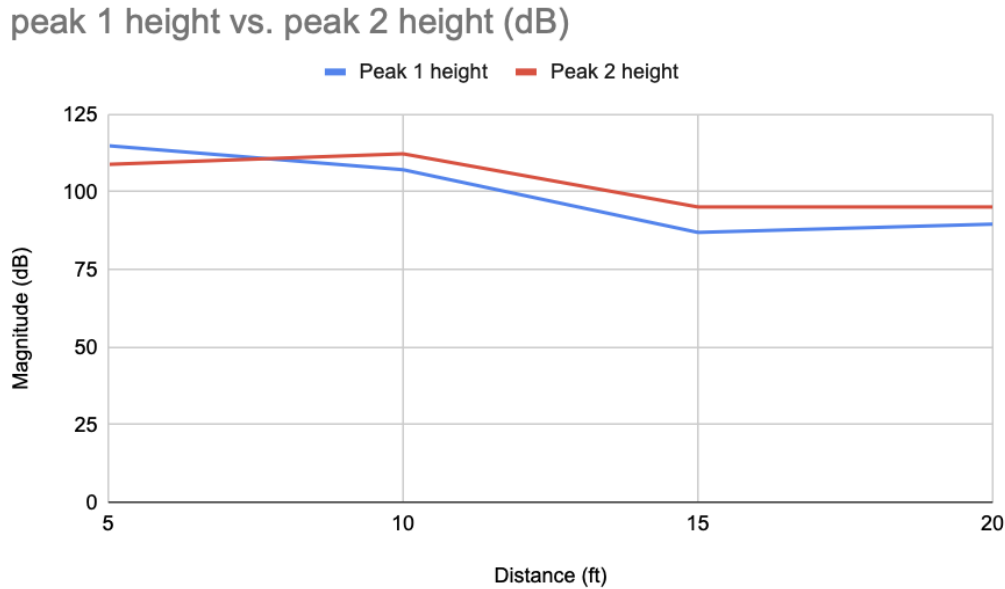


Figure 21. Peak 1 vs Peak 2 over distance.

In the control tests, the radar was off by an average of 3%. This error can be attributed to improper sign spacing more than an error in the radar board itself. In setting up the experiments, a tape measure was used as the true distance that the radar signature was compared to. The true spacing was probably within inches of what the tape measure recorded. Consistent bias would raise suspicion about the radar's accuracy, but small fluctuations are likely human error.

As the distance from the sign increases, the magnitudes of the reflected waves generally decrease. There was a clear trend for the peak magnitude for this data. In random scanning for a hollow street sign, a double peak matching these lines would give confidence that it has been found. Given a sign is located, the car will track it down to find the distance within about 5%. Also, the signs are more precise than they are accurate. Therefore, they can be calibrated to give more accurate data and decrease the distance percent error.

peak 1 height vs. peak 2 height (dB) at 10 feet

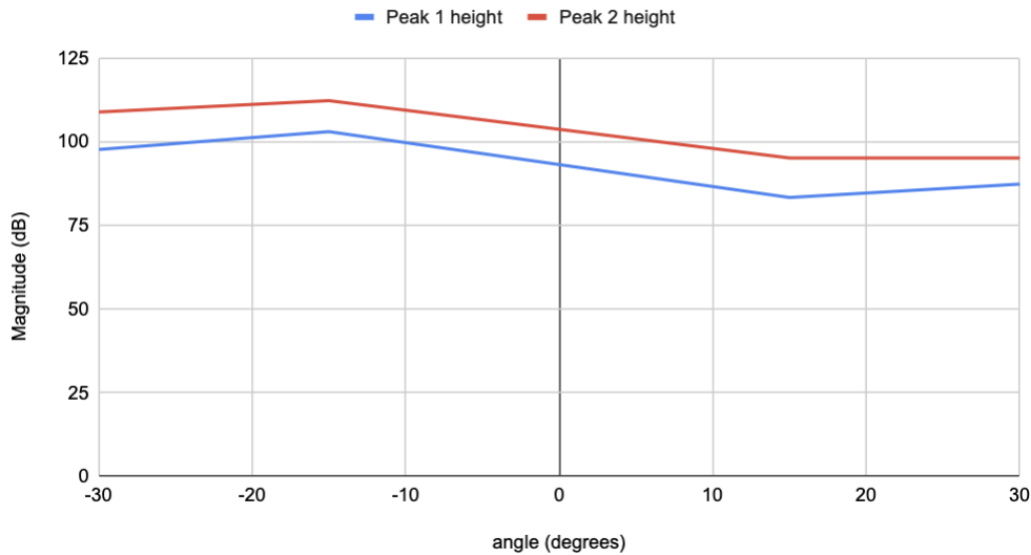


Figure 22. Peak 1 vs. Peak 2 at 10 feet over different angles at 10 feet.

Weather Testing

Snow Testing

Table 11. Snow conditions.

| Distance (feet) | Peak 1 Mean \pm CI (dB) | Δ vs 0° P1 (dB) | Peak 2 Mean \pm CI (dB) | Δ vs 0° P2 (dB) | $ Loc P1 $ Mean Error (ft) | $ Loc P2 $ Mean Error (ft) |
|-----------------|---------------------------|-------------------------------|---------------------------|-------------------------------|----------------------------|----------------------------|
| 10 | 108.3 ± 3.2 | 1.2 | 100.8 ± 5.0 | -11.4 | 0.2 | 1.1 |
| 15 | 108.3 ± 0.9 | 21.3 | 102.0 ± 0.2 | 6.9 | 0.2 | 1.0 |
| 20 | 104.5 ± 0.9 | 14.9 | 109.4 ± 0.8 | 14.3 | 1.0 | 0.4 |

Means \pm 95% CI; Deltas are relative to the 0° control; Location error = measured distance - true distance.

Snow testing shows the sign's consistent two-peak radar signature at all three ranges and maintains range estimates. At 10 feet and 15 feet, mean absolute distance errors remain small, about 0.16 feet for Peak 1 and 1.0-1.1 feet for Peak 2. This is consistent with the control group and confirms that location is stable even as weather changes. Peak magnitudes at these distances stay about, demonstrating a large detectability margin in falling snow. At 20 feet, both peaks are still clearly detected, and the mean absolute distance errors present a systematic offset, rather

than random loss. Overall, snow reduces signal margin at longer range but does not suppress the signature or ability to estimate distance, supporting the main claim that the hollow sign remains machine-readable in adverse weather conditions.

Rain Testing

Table 12. Rain Conditions

| Distance (feet) | Peak 1 Mean ± CI (dB) | Δ vs 0° P1 (dB) | Peak 2 Mean ± CI (dB) | Δ vs 0° P2 (dB) | Loc P1 Mean Error (ft) | Loc P2 Mean Error (ft) |
|--------------------|-----------------------------|--------------------|-----------------------------|--------------------|-------------------------------|-------------------------------|
| 10 | 109.2 ± 0.7 | 2.0 | 99.8 ± 0.4 | -12.5 | 1.1 | 1.7 |
| 15 | 98.8 ± 0.6 | 11.8 | 103.8 ± 0.0 | 8.7 | 0.7 | 0.1 |
| 20 | 97.1 ± 0.7 | 7.5 | 99.8 ± 0.4 | 4.7 | 0.4 | 1.1 |

Means ± 95% CI; Deltas are relative to the 0° control; Location error = measured distance - true distance.

The rain interfered with the radar a bit more than the snow did at 10 ft, but less at 15 ft. Importantly, the sign was able to clearly maintain 2 peaks from the sign, and it was able to accurately measure the distance from the sign.

Fog Testing

Table 13. Fog Conditions

| Distance (feet) | Peak 1 Mean ± CI (dB) | Δ vs 0° P1 (dB) | Peak 2 Mean ± CI (dB) | Δ vs 0° P2 (dB) | Loc P1 Mean Error (ft) | Loc P2 Mean Error (ft) |
|--------------------|-----------------------------|--------------------|-----------------------------|--------------------|-------------------------------|-------------------------------|
| 10 | 114.4 ± 0.7 | 7.2 | 105.4 ± 0.4 | -6.9 | 1.2 | 2.0 |
| 15 | 105.7 ± 0.8 | 18.8 | 96.55 ± 1.2 | 1.4 | 0.1 | 0.9 |
| 20 | 106.2 ± 0.4 | 16.6 | 109.3 ± 0.7 | 14.2 | 1.1 | 0.4 |

Means ± 95% CI; Deltas are relative to the 0° control; Location error = measured distance - true distance.

The Radar was the most accurate both in terms of the distance measured and the magnitude of the signal at 15 ft. This makes sense because light in the radar range isn't affected by fog, and it is clear to it since fog doesn't disrupt those wavelengths of light.

Radar Overview

Finally, we can compare how the different weather conditions perform against each other and our control, to get an understanding of how well the radar performs as a replacement for traditional sensors on self-driving vehicles.

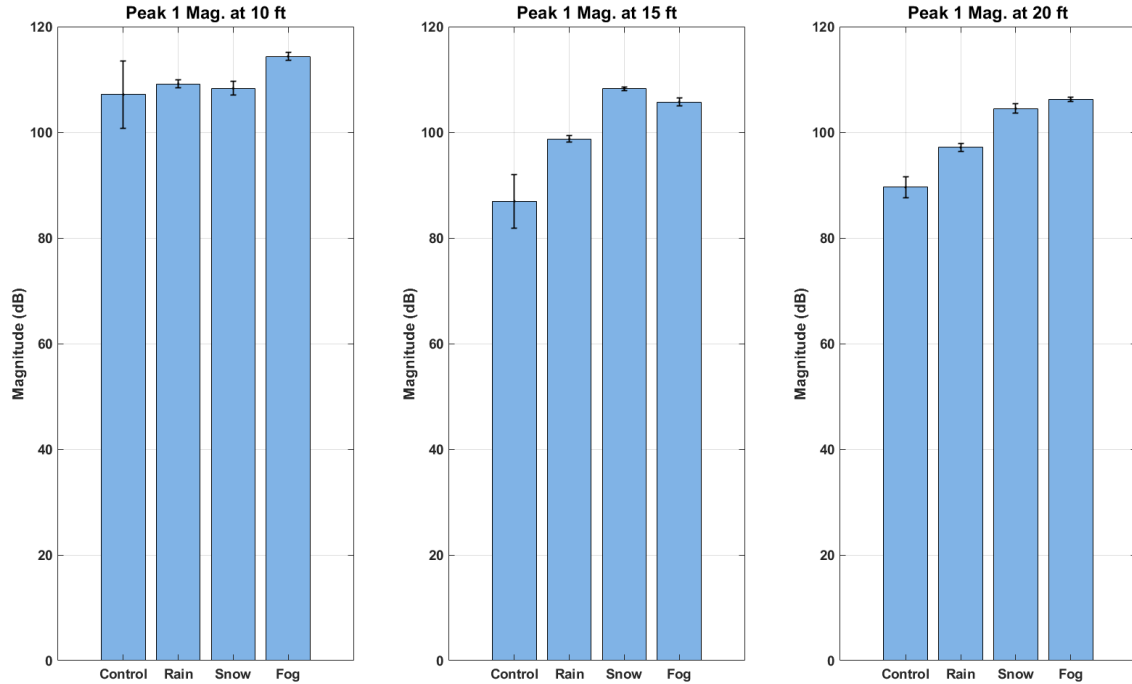


Figure 23. Average peak 1 magnitudes at each distance

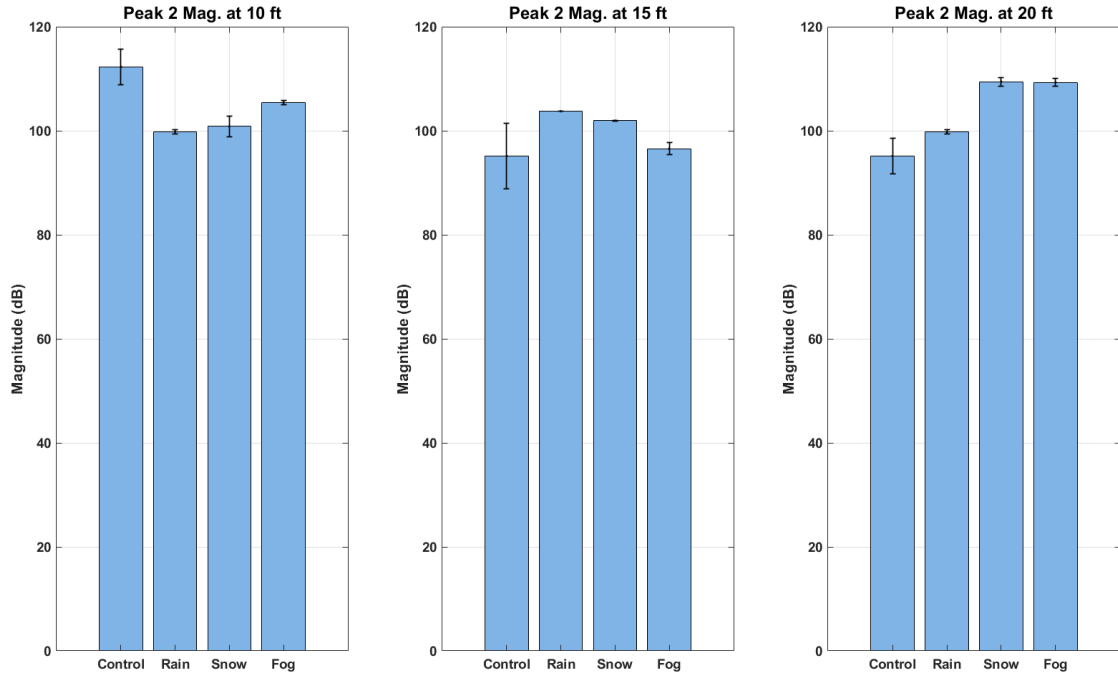


Figure 24. Average peak 2 magnitudes at each distance

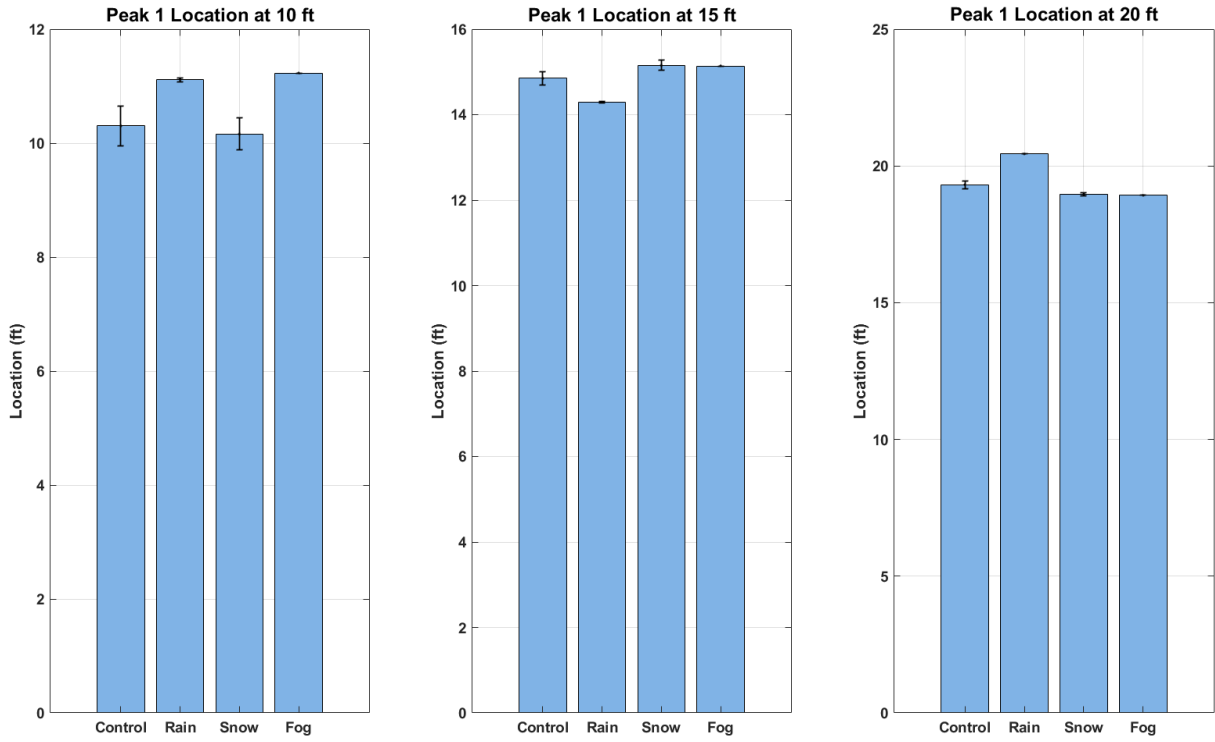


Figure 25. Average peak 1 location for each distance

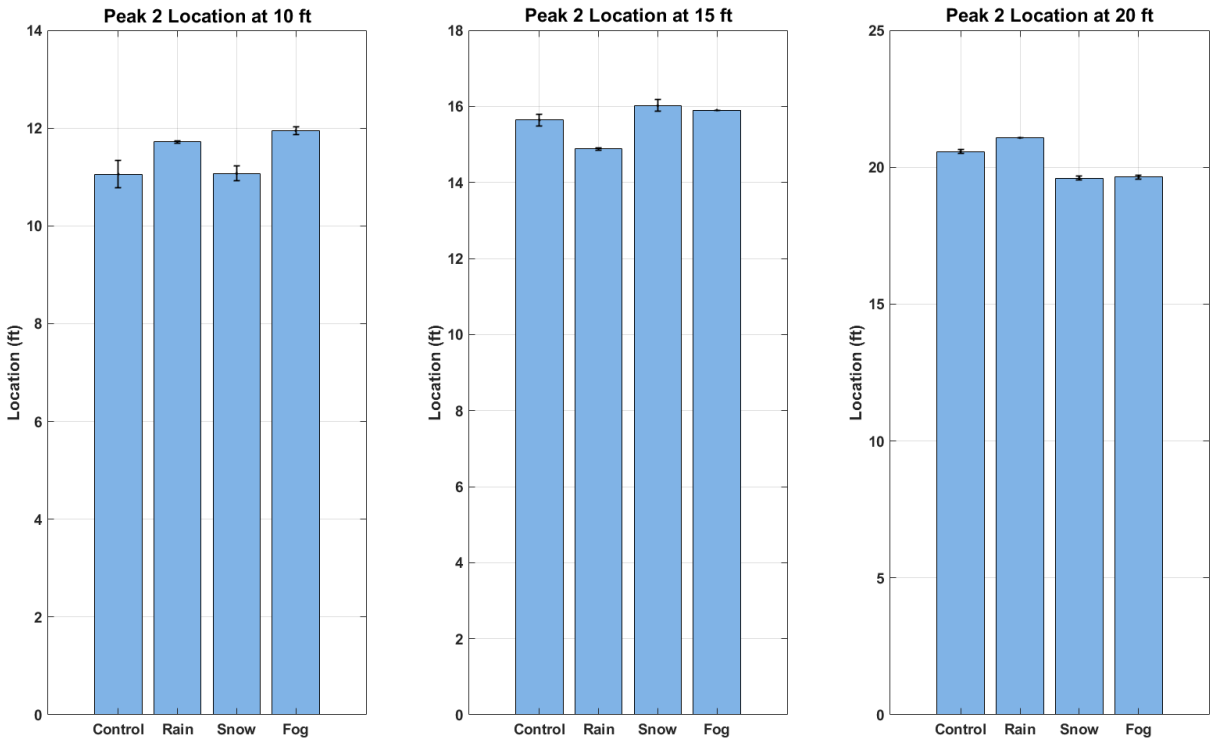


Figure 26. Average peak 2 location for each distance

Comparing the different results side by side, we see they all perform roughly the same as the control. Interestingly, our rain data has almost no difference in the repeated tests; however, it affected the measured distance of the sign the most. Looking at the magnitude plots, again, the rain messed with the sensor the most in all of the tests, except for peak 1 at 15 ft, where it was snow that had the greatest impact. It should be noted, though, that our project used one of the cheapest radars we could find in order to still have some budget for the rest of our project, and the radar camera in autonomous vehicles will almost certainly be much more accurate. However, even with our cheap radar, it was able to see through fairly reliably. For the first peak, distance errors were generally within about a foot, and even the secondary peak stayed within about 2 feet, and more importantly, it was able to consistently get two peaks off of the sign, with the difference between the two also being consistent.

Upon project initiation, the most critical user needs were improved autonomous vehicle safety in poor weather, accurate terrain mapping, affordability, and reliability. This research gives confidence that this sign geometry provides critical location information to autonomous vehicles in situations where their current technology fails. Therefore, it has the potential to increase their safety and reliability. Through project development, terrain mapping, and cost were removed from the project scope. Implementation procedures and cost would be considered after more comprehensive testing because installing these signs along roads would be a huge construction undertaking. Terrain mapping is outside the scope of using radar signatures to locate vehicles.

Several ANOVA tests will compare the critical values of different conditions. The ANOVA test assumes that the samples are independent, the data in each group are approximately normally distributed, and that the variances across groups are equal (homoscedasticity). The p-value output has the possibility of disproving the null hypothesis: The true mean between the groups is the same. They will compare the magnitude of the first peak for each distance. Then for the second peak. Lastly, it will compare the difference in peak location between all the groups.

Table 14. ANOVA test p-val comparing peak heights under conditions at various distances

| | Peak 1 | Peak 2 |
|-------|----------|----------|
| 10 ft | 0.105 | 0.00024 |
| 15 ft | 4.37 E-5 | 0.03033 |
| 20 ft | 4.59 E-7 | .0000212 |

Five out of the six ANOVA tests run fail a confidence level of 5%. This disproves the null hypothesis that the true means are the same. It therefore proves inclement weather impacts the magnitude of the radar graphs. This is further supported by the bar graphs in figure 23 and 24

where the average magnitudes are displayed. In general, the impaired conditions produced higher magnitude readings than the control group.

The next ANOVA tests compare the difference between the peaks for each distance. The null hypothesis is that weather conditions do not affect the distance between the peak and the true value is constant between groups.

Table 15. ANOVA test p-val comparing peak location differences under conditions at various distances

| | Peak distance difference |
|-------|--------------------------|
| 10 ft | .0264 |
| 15 ft | 8.13 E-7 |
| 20 ft | 0.209 |

Two out of the 3 ANOVA tests fail with a confidence level of 5%. These reject the null and prove weather impacts the distance between the peaks at distances 10 and 15 feet. At 20 feet, the p-val 0.209 is not enough to disprove the null hypothesis and supports the goal of the project. In practice, the radar readings will usually be greater than 20 feet from the sign, so the distance between peaks has an expected value regardless of weather conditions.

Statistical analysis proved weather conditions affect radar readings but do not impair them entirely. Their data is useful in detecting the distance to the sign. Unique feature metrics would need to be tailored for distances and weather conditions. If a car knows it is snowing, it would reference internal data and compare its metrics to graphs at similar distances to fully evaluate if the image is coming from a sign. Then, it would pull the distance value if the sign is verified. The distances were shown to be reliable and accurate.

LiDAR Evaluation

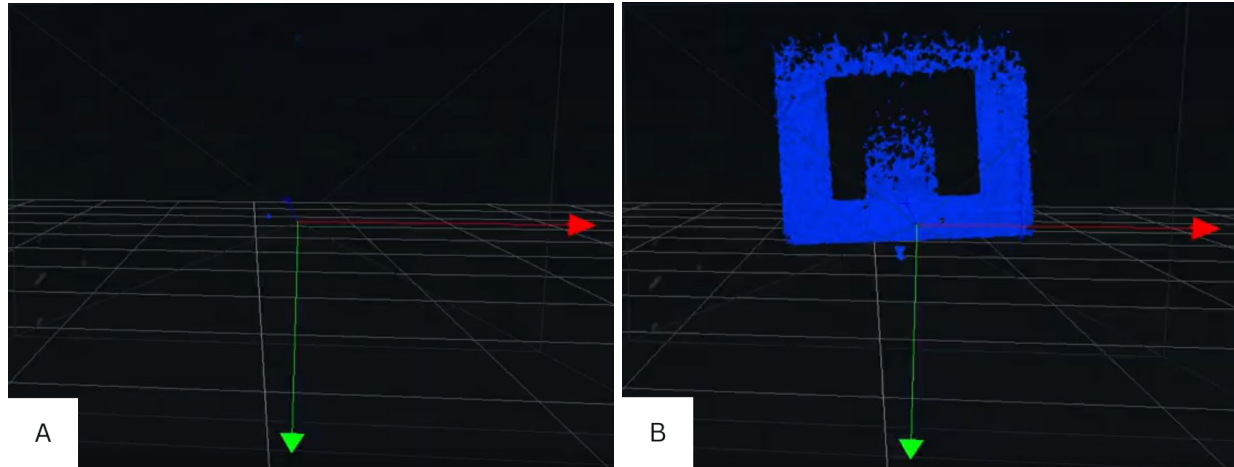


Figure 27. (A) LiDAR's reaction after fog is presented before the sensor and the sign. (B) The sign became more apparent after the fog dissipated.

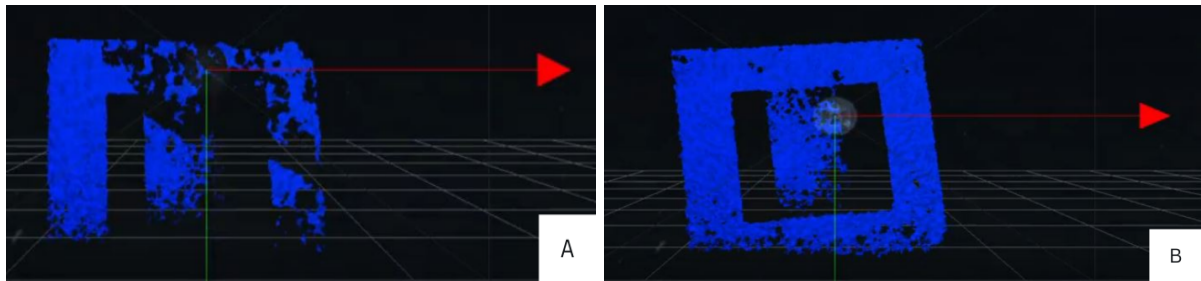


Figure 28. (A) LiDAR's loss of image of the sign due to a simulated snowstorm. (B) The same sign became more apparent after the snow cleared up.

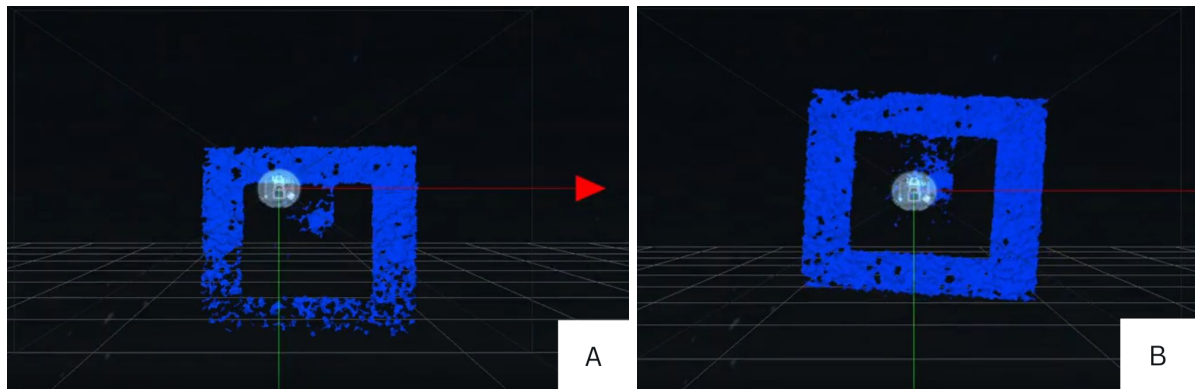


Figure 29. (A) LiDAR still shows the presence of the sign's outline during a rainstorm. (B) The sign begins to reappear after the rain starts to ease up.

The results from the LiDAR figures demonstrate the various weather conditions on LiDAR systems and their ability to detect and render objects in the environment. As fog was introduced between the sensor and the sign, the LiDAR point cloud began to deteriorate. This was due to increased scattering and absorption of the emitted laser pulses. As shown in Figure 27

(A), the presence of fog significantly reduces the visibility of the sign. Once the fog dissipated, the LiDAR regained visual access to the structure, and the sign's shape became more distant, further illustrated in Figure 27 (B). This shows that LiDAR fails in extremely foggy conditions as it scatters the particles so that the sign no longer becomes apparent.

During the simulated snowy environment, the reduction became more and more apparent as more snow particles began to cover up the sign. Snowflakes work as reflective interference points, causing the sensor to lose large portions of the sign's outline. Instead of returning a clean image of the sign, certain segments begin to disappear from view. As more and more of the sign begin to disappear, the failure points of the LiDAR system begin to become more apparent. From this example, this was caused by a snow machine that could only expel a small amount of snow at a time, and it was able to disrupt the photo of the sign overall. These observations confirm that snow introduces stronger occlusions than fog, which can lead to more severe losses in point-cloud accuracy.

In rainy conditions, the effects were noticeable but not as disruptive as snow and fog. The LiDAR remained capable of detecting the main outline of the sign with slight disturbances due to scattered points and noise in the scene. Water droplets still interfered with some of the returning beams, but the structure remained at least partially visible throughout the testing. AS the rainfall eased, the point cloud quality improved, clearly recovering the sign's shape. This indicates that rain introduces measurement noise and partial occlusion, and the system can still maintain a reasonable level of detection reliability.

Overall, the experiments highlight a clear trend that atmospheric disturbances that introduce dense, reflective particles, such as fog and snow, cause the greatest degradation of LiDAR object detection. Rain allowed for a persistent object with visible noise that disturbs the picture of the sign. These results emphasize the importance of environmental algorithms and sensor fusion combining LiDAR and radar systems to maintain a reliable and safe perception in adverse weather conditions.

Radar Application to Location

The purpose of these signatures is to detect the signs uniquely and attain distance readings. Above calculations outline the efficiency of detecting a sign and gathering an accurate distance value.

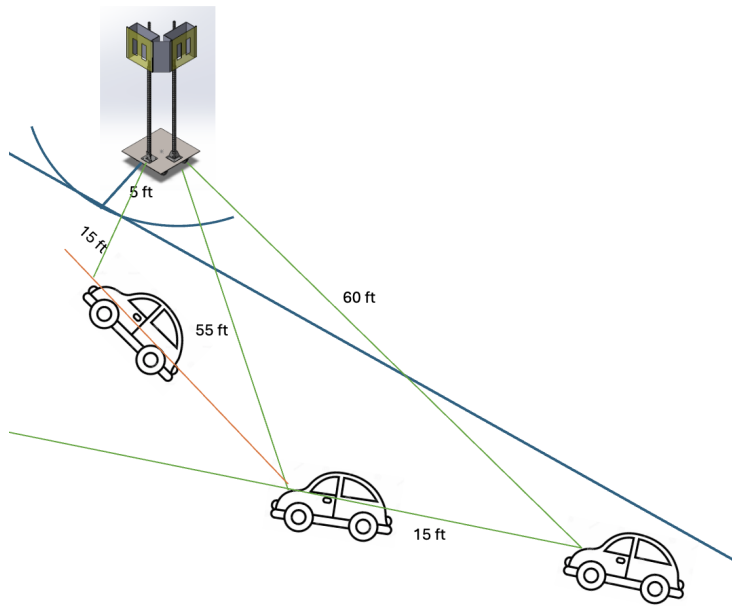


Figure 30. Schematic of radar mapping example

Given two distances and the distance traveled by the car, the law of cosines will find the angle between the path the car is traveling and the direction to the sign. It will then point towards or away from the sign. If the distance traveled equals the change in distance readings, the car is headed straight towards the sign, so it should turn slightly left. This assumes the signs are always located on the right side of the road. Implementation would require standardized spacing from the road side.

Limitations

The current results were collected in a controlled environment with constructed weather equipment (fog machine, snow machine, rain hose) and a relatively uncluttered background. This is an advantage when attempting to maintain the controlled variables and prove cause-and-effect relationships, but it's not the same as a real road scene with messy precipitation, reflective clutter (cars, puddles, etc), or the sensor and sign moving relative to each other. Due to that, more variance should be expected in the field compared to the lab.

Several conditions currently include three trials. These are useful for trend assessment, but expanding replication to five trials per condition is recommended to narrow confidence intervals, improve stability, and support more decisive comparisons across conditions. Possible sources of error include:

- Alignment (systematic bias): small variations in angle can bias peak locations and magnitudes.
- Multipath and background visibility (random variance): unmodeled reflectors add noise and other peaks.

- Precipitation density variability (random variance): fog, snow, and rain intensity are not perfectly uniform across all trials.

Attempts to decrease the possibility of error were used, including angle adjustment, standard radar settings, and fixed sensors. To strengthen validity in future tests, complete at least five trials per condition, add at least one cluttered background condition (representing a road scene), include a low-speed motion test to assess stability, and measure weather intensity levels to compare performance in each condition. Collectively, these steps will increase the robustness and usability of the results.

Error

Over the course of two semesters of experimentation, several challenges arose in testing and collecting radar data, each requiring iterative adjustments to the procedures. The most common issues involved unwanted noise in the radar readings, unexpected returns where no physical objects were present, and difficulty ensuring that simulated weather conditions matched the density and behavior of real-world environments.

The primary source of potential error came from inconsistent noise levels in the radar sensor output, including occasional peaks appearing only centimeters from the sensor. These fluctuations made it harder to distinguish true signal peaks from surrounding interference and required careful control of the testing environment to eliminate debris or unintended reflectors. Weather-related testing also introduced uncertainty. Because of limited time and resources, harsh weather conditions had to be simulated only in the immediate space in front of the radar rather than across the entire sign-to-sensor distance. Although this approach was the most practical under the constraints, a more ideal setup would have fully immersed the complete measurement range within the simulated conditions.

Throughout planning and execution, these potential sources of error were recognized and mitigated as much as possible. Procedures were refined to ensure consistent, repeatable testing, particularly during weather simulations, where an enclosure was built to increase particulate density and better observe its effects on returned signals. Despite these efforts, some amount of uncertainty in the data is still expected. The accompanying uncertainty analysis is therefore essential for explaining deviations between test conditions and expected results.

Impact

These results, as hoped, show that radar sensors are capable of providing clean and accurate data through several of the harshest and difficult driving conditions. In cases of extreme snow, rain, or fog, a human may not be able to safely navigate a highway or drive along the side of a cliff's edge, but proof shows that with the aid of the presented sign design, it may be possible to provide helpful driving information to an autonomous vehicle to prevent a serious incident from occurring. A goal of autonomous vehicle implementation into present and future society is

to reduce the number of vehicular-based injuries and fatalities. While this design may not provide support in vehicle-to-vehicle-based accidents, it does aim to prevent those accidents that may be a consequence of poor visibility and lead to potential harm due to uncertain road conditions. This design strives to provide more information to a vehicle to allow it to make the correct choices when turning a mountainside corner in heavy snow or coming across new construction on a remote highway. As autonomous vehicles evolve in design, this project hopes to innovate on the tools available on the roadside and provide the most detailed information available for times in which standard cameras or LiDAR sensors may fail to recognize impending dangers. The data provided here and the results derived from it are proof that this project may be able to provide unique value to the world of driving and level 5 AVs by making roadways safer by giving those vehicles the most information possible to make the right choice and ultimately improve the safety of every individual who may find themselves on the roadway.

Conclusion

Continued development of the current prototype could entail several alterations and improvements, along with further testing to provide even greater support for the claims made in this document. Changes or improvements would include further adaptations of the sign face and orifice, as the main interest is to create a Radar signature that is both unique and prominent within the overall return seen from the Radar. Several possible alterations could be a change in size of the sign or the pattern over the orifice to improve the magnitude of the returning signal. A secondary goal of this project was to possibly create multiple sign iterations that would produce unique signatures of their own to portray different translations to an autonomous vehicle, which would allow these signs to be used in multiple applications and locations across the globe. In order to do this, alterations to the design of the orifice would need to be made to create these aforementioned unique signatures, and with further testing and design changes, multiple prototypes could be produced to test this theory. Other design changes that are possible are the material selection, as currently the sign is made of steel, which allows for the Radar signals to reflect and return to the sensor, but it may be possible that other materials are more cost-effective with similar results or better. Similar to the material choice of the sign, the stand could be reimagined to allow for it to be secured into the ground either with concrete or bolts, as well as the selection of materials, as it is currently being supported by perforated steel, which could be replaced by something of the likes of unistrut.

Testing procedure throughout the course of the year has yielded positive results; however more could always be done. The three weather conditions tested were snow, rain, and fog; however many more exist, of course. In Southwestern states, it may be beneficial to test in conditions such as during a dust storm due to their frequency, as well as hail. These weather conditions vary from what was tested, as sand and hail are often much larger solid particulates than snow and may potentially interrupt outgoing Radar signals. Other testing that could have provided improved results would be, as mentioned previously, the material selection of the sign. It was found in testing that the Radar signal completely penetrated the cardboard housing the fog, whereas it reflected with some magnitude off the steel sign. There may be other materials that could be tested for their reflectivity and application in this product, as it may further extend the magnitude of the returned signal, differentiating it from any other surrounding objects. Further testing was completed, the sign would then be prepared for production and implementation on highways across the United States. In order for this foundational change to the roadways of the Nation, certain permissions would need to be granted and possibly approved by local or national authorities. These entities would include the Federal Highway Administration (FHWA) as well as local authorities such as the Arizona Department of Transportation (ADOT) for installation and maintenance of these signs. Production would include the purchasing of the material for the sign as well as the machining of the face and formation of the body. Stands from current street signs could be easily used as well for these and cemented into the ground on highways for permanent use. To take this product even further, it would require the attention of such

authorities and the selection of manufacturing plants mainly, and other responsibilities could include the distribution of the signs and sales.

References

- [1] A. Bole, A. Wall, and A. Norris, “Radar Cross section,” Radar Cross Section - an overview | ScienceDirect Topics, <https://www.sciencedirect.com/topics/engineering/radar-cross-section> (accessed Mar. 16, 2025).
- [2] “Addressing challenges for autonomous vehicles on Winter Roads,” Addressing Challenges for Autonomous Vehicles on Winter Roads | Center for Transportation Studies, <https://www.cts.umn.edu/research/featured/futureofmobility/rajamani#:~:text=In%20addition%20to%20this%20fundamental,current%20is%20also%20very%20difficult>. (accessed Sep. 21, 2025).
- [3] C. Wolff, “Radar basics,” Radartutorial, <https://www.radartutorial.eu/01.basics/Distance-determination.en.html> (accessed Mar. 16, 2025).
- [4] E. Ackerman, “What full autonomy means for the waymo driver,” IEEE Spectrum, <https://spectrum.ieee.org/full-autonomy-waymo-driver> (accessed Sep. 21, 2025).
- [5] Impact of speeds on drivers and vehicles — results from ..., <https://aaafoundation.org/wp-content/uploads/2021/01/Impact-of-Speeds-on-Drivers-and-Vehicles-Results-from-Crash-Tests.pdf> (accessed Mar. 17, 2025).
- [6] iStockphoto, “Snow Covered Traffic Sign Road,” iStockphoto. [Online]. Available: <https://media.istockphoto.com/id/485627214/photo/snow-covered-traffic-sign-road.jpg?s=612x612&w=0&k=20&c=3qDKUlfQgKx0cguRYdY27QCBGVY4pTlkdc0HZYHTgXw=> [Accessed: Mar. 16, 2025].
- [7] J. Dedvukaj, “Are self-driving cars safe? GM cruise lawsuit raises concerns,” The Joseph Dedvukaj Firm, P.C, <https://www.1866hirejoe.com/blog/the-road-ahead-are-self-driving-cars-safe/> (accessed Sep. 21, 2025).
- [8] K. Ramasubramanian, “MmWave radar for automotive and Industrial Applications,” ti, https://www.ti.com/content/dam/videos/external-videos/en-us/2/3816841626001/5675916489001.mp4/subassets/Mmwave_webinar_Dec2017.pdf (accessed Mar. 16, 2025).
- [9] L. Lowery, “GM using AI in manufacturing and advancing toward level 3 autonomy on the road,” Repairer Driven News, <https://www.repairerdrivennews.com/2025/03/13/gm-using-ai-in-manufacturing-and-advancing-toward-level-3-autonomy-on-the-road/> (accessed Sep. 21, 2025).
- [10] M. Tung, Tesla autopilot | explore our blog | jameco electronics, <https://www.jameco.com/Jameco/workshop/HowItWorks/how-it-works-tesla-autopilot-self-driving-automobile-technology.html> (accessed Sep. 22, 2025).
- [11] “Maximum allowable stress,” Maximum Allowable Stress - an overview | ScienceDirect Topics, <https://www.sciencedirect.com/topics/engineering/maximum-allowable-stress> (accessed Mar. 16, 2025).
- [12] Owner’s Manual | Tesla, <https://www.tesla.com/ownersmanual> (accessed Sep. 22, 2025).

- [13] “Radar Equation,” MathWorks,
<https://www.mathworks.com/help/radar/ug/radar-equation.html> (accessed Mar. 16, 2025).
 - [14] “Self-driving car technology for a reliable ride - Waymo Driver,” Waymo,
<https://waymo.com/waymo-driver/> (accessed Sep. 21, 2025).
 - [15] Study.com, “Heat of Fusion: Definition, Equation, Examples,” Study.com. [Online]. Available:
<https://study.com/academy/lesson/heat-of-fusion-definition-equation-examples.html#:~:text=The%20latent%20heat%20of%20the%20fusion%20of%20water%20is%20equal,water%20from%20solid%20to%20liquid.> [Accessed: Mar. 16, 2025].
- [16] U.S. Department of Transportation, “III. Sign Materials,” Federal Highway Administration. [Online]. Available:
<https://highways.dot.gov/safety/local-rural/maintenance-signs-and-sign-supports/iii-sign-materials#:~:text=Aluminum%20is%20by%20far%20the,andaluminum%20is%20lighter%20than%20aluminum.> [Accessed: Mar. 16, 2025].
 - [17] “User’s Guide SWRU529C–May 2017–Revised April 2020 mmWave Demo Visualizer,” Ti,
https://www.ti.com/lit/ug/swru529c/swru529c.pdf?ts=1720599732929&ref_url=http%253A%252F%252F127.0.0.1%253A58091%252F (accessed Nov. 24, 2025).
 - [18] “What is Young’s modulus of steel?,” Buy steel online at steeloncall.com,
<https://steeloncall.com/what-is-young-s-modulus-of-steel#:~:text=Young's%20modulus%20of%20steel%20at,underneath%20as%20far%20as%20possible.> (accessed Mar. 16, 2025).
- [19] Wikimedia Commons, “Back of street signs,” Available:
https://upload.wikimedia.org/wikipedia/commons/7/7b/Back_of_street_signs.jpg [Accessed: Mar. 16, 2025].

| Parameter | Value | Units | Type | Description |
|--------------------------------------|----------|-------------------------------------|------------|---|
| Snowfall Rate (input) | 1.2 | in/hr | user input | Moderate snowfall rate in inches per hour. |
| 1 inch → meters | 0.0254 | m/in | constant | Conversion factor from inches to meters. |
| 1 hour → seconds | 3600 | s/hr | constant | Conversion factor from hours to seconds. |
| Snowfall Velocity | 8.50E-06 | m/s | calculated | Converts snowfall rate from in/hr to m/s. |
| Sign Area | 0.5 | m ² | user input | Surface area of the sign. |
| Snow Density | 200 | kg/m ³ | user input | Approximate density of moderately packed snow. |
| Volumetric Flow Rate | 4.25E-06 | m ³ /s | calculated | Snowfall volume hitting the sign per second. |
| Mass Flow Rate | 8.50E-04 | kg/s | calculated | Snow mass hitting the sign per second. |
| Latent Heat of Fusion (constant) | 334000 | J/kg | constant | Energy required to melt 1 kg of snow/ice. |
| Specific Heat of Ice | 2100 | J/kg | constant | Energy required to raise 1 kg of ice by 1 °C before melting |
| Heat to Warm Snow | 17.8 | W | calculated | Power needed to warm incoming snow. (1 W = 1 J/s) |
| Heat to Melt Snow | 2.84E+02 | W | calculated | Power needed to melt incoming snow. (1 W = 1 J/s) |
| Convective Heat Transfer Coefficient | 25 | W/(m ² ·K) | user input | Assumed for moderate wind conditions. |
| Sign Temperature (input) | 277 | K | user input | Desired sign surface temperature (4 °C). |
| Ambient Temperature (input) | 263 | K | user input | Outside air temperature (-10 °C). |
| Convective Heat Loss | 175 | W | calculated | Heat lost via convection. |
| Emissivity (constant or input) | 0.8 | — | constant | Emissivity of the sign surface (typical for painted metal). |
| Stefan–Boltzmann Constant | 5.67E-08 | W/(m ² ·K ⁴) | constant | Physical constant for blackbody radiation. |
| Radiative Heat Loss | 2.50E+01 | W | calculated | Heat lost via thermal radiation. |
| Total Heat Required | 5.02E+02 | W | calculated | Sum of snow melting, convection, and radiation power. |

6.d

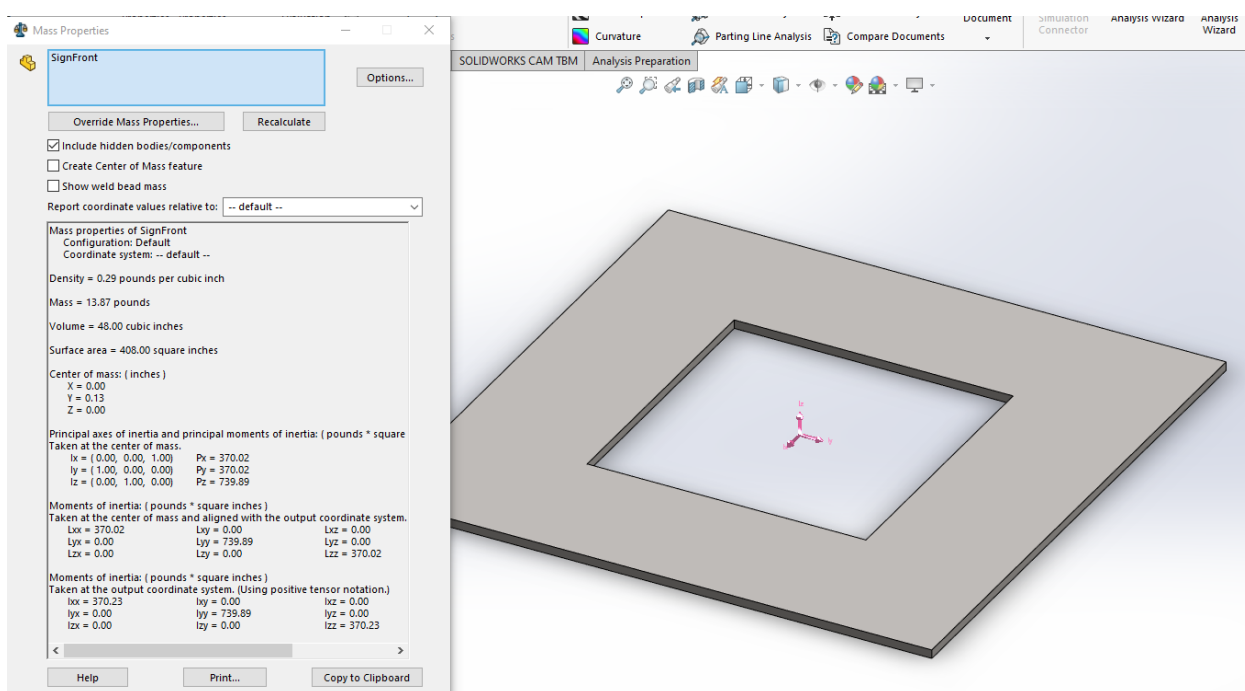
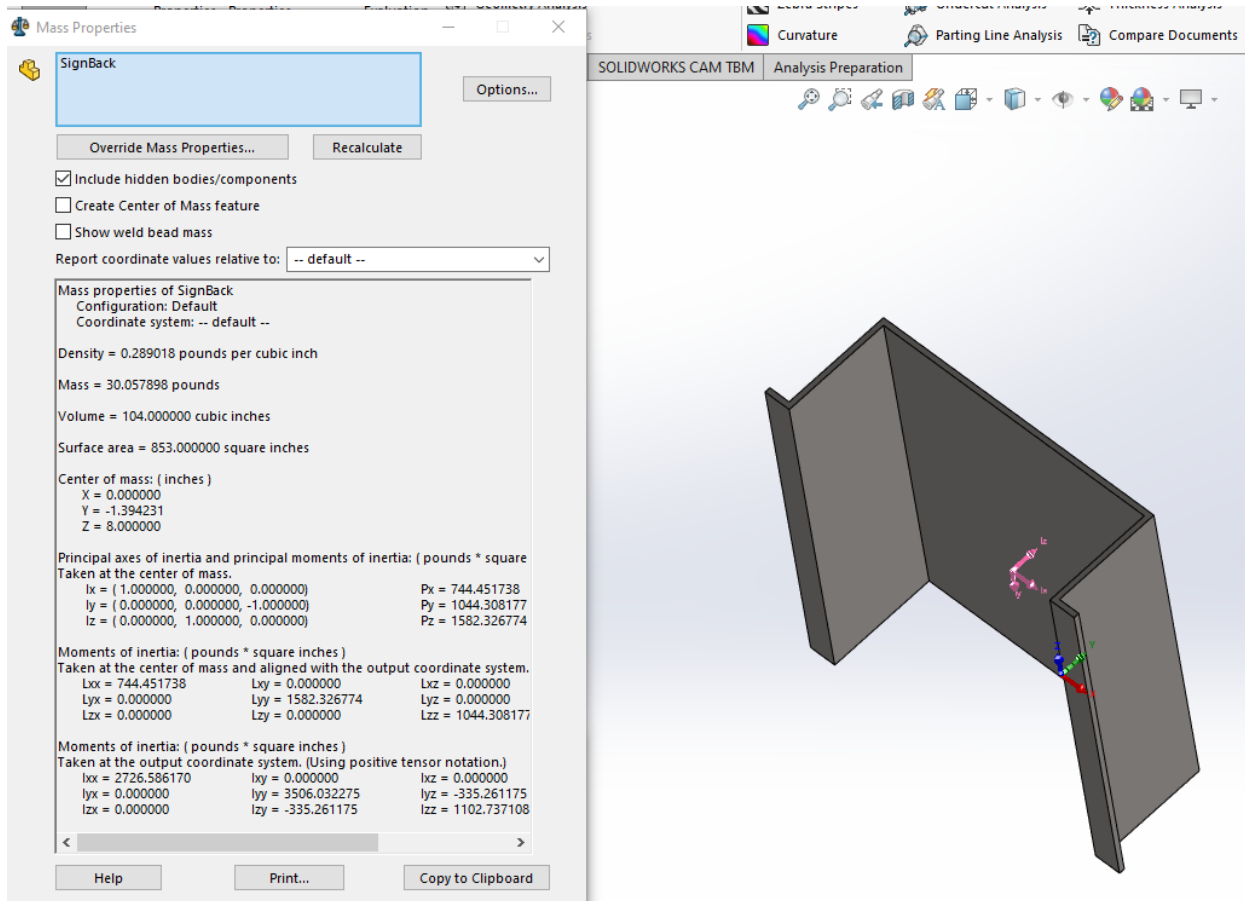
Material Properties Used for design modeling

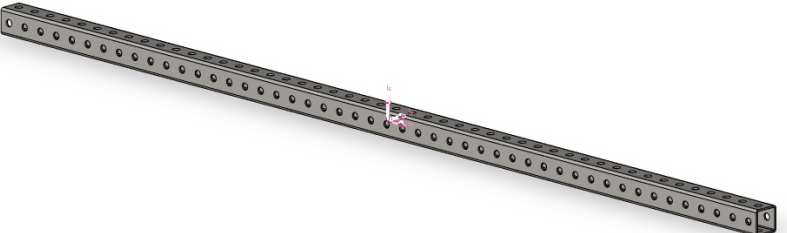
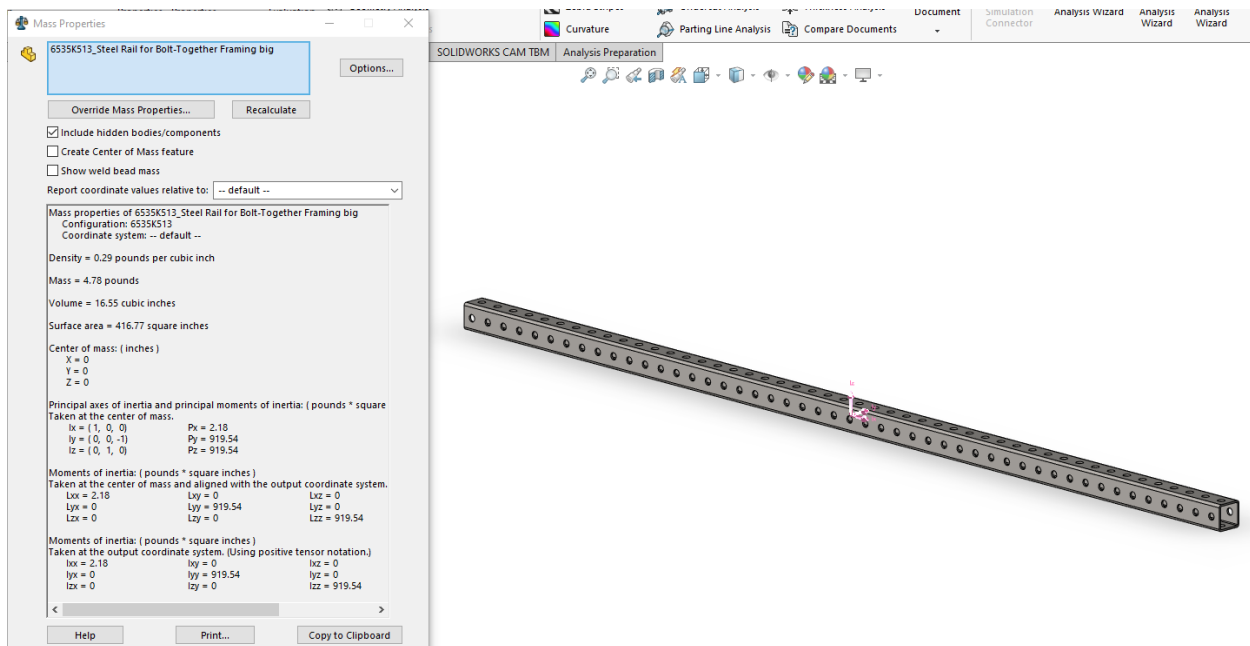
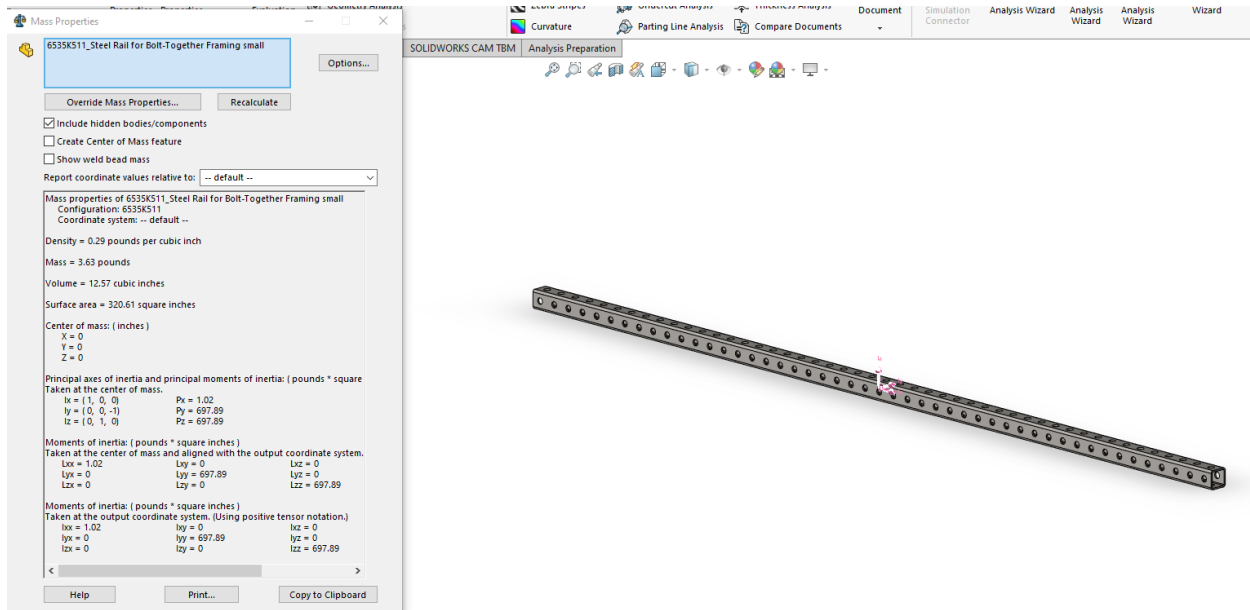
Material properties

Materials in the default library can not be edited. You must first copy the material to a custom library to edit it.

| | | |
|----------------------------|--------------------------|---|
| Model Type: | Linear Elastic Isotropic | <input type="checkbox"/> Save model type in library |
| Units: | English (IPS) | |
| Category: | Steel | |
| Name: | AISI 304 | |
| Default failure criterion: | Max von Mises Stress | |
| Description: | | |
| Source: | | |
| Sustainability: | Defined | |

| Property | Value | Units |
|-------------------------------|--------------|-----------------|
| Elastic Modulus | 27557170.16 | psi |
| Poisson's Ratio | 0.29 | N/A |
| Shear Modulus | 10877830.32 | psi |
| Mass Density | 0.2890182545 | lb/in^3 |
| Tensile Strength | 74986.97601 | psi |
| Compressive Strength | | psi |
| Yield Strength | 29994.81941 | psi |
| Thermal Expansion Coefficient | 1e-05 | /°F |
| Thermal Conductivity | 0.000213996 | Btu/(in·sec·°F) |





Unified Threads (UNC and UNF)

| Size Designation | Nominal Major Diameter in | Coarse Series—UNC | | | Fine Series—UNF | | |
|------------------|---------------------------|--------------------|--|--|--------------------|--|--|
| | | Threads per Inch N | Tensile-Stress Area A, in ² | Minor-Diameter Area A, in ² | Threads per Inch N | Tensile-Stress Area A, in ² | Minor-Diameter Area A, in ² |
| 0 | 0.0600 | | | | 80 | 0.001 80 | 0.001 51 |
| 1 | 0.0730 | 64 | 0.002 63 | 0.002 18 | 72 | 0.002 78 | 0.002 37 |
| 2 | 0.0860 | 56 | 0.003 70 | 0.003 10 | 64 | 0.003 94 | 0.003 39 |
| 3 | 0.0990 | 48 | 0.004 87 | 0.004 06 | 56 | 0.005 23 | 0.004 51 |
| 4 | 0.1120 | 40 | 0.006 04 | 0.004 96 | 48 | 0.006 61 | 0.005 66 |
| 5 | 0.1250 | 40 | 0.007 96 | 0.006 72 | 44 | 0.008 80 | 0.007 16 |
| 6 | 0.1380 | 32 | 0.009 09 | 0.007 45 | 40 | 0.010 15 | 0.008 74 |
| 8 | 0.1640 | 32 | 0.014 0 | 0.011 96 | 36 | 0.014 74 | 0.012 85 |
| 10 | 0.1900 | 24 | 0.017 5 | 0.014 50 | 32 | 0.020 0 | 0.017 5 |
| 12 | 0.2160 | 24 | 0.024 2 | 0.020 6 | 28 | 0.025 8 | 0.022 6 |
| $\frac{1}{4}$ | 0.2500 | 20 | 0.031 8 | 0.026 9 | 28 | 0.036 4 | 0.032 6 |
| $\frac{5}{16}$ | 0.3125 | 18 | 0.052 4 | 0.045 4 | 24 | 0.058 0 | 0.052 4 |
| $\frac{3}{8}$ | 0.3750 | 16 | 0.077 5 | 0.067 8 | 24 | 0.087 8 | 0.080 9 |
| $\frac{7}{16}$ | 0.4375 | 14 | 0.106 3 | 0.093 3 | 20 | 0.118 7 | 0.109 0 |
| $\frac{1}{2}$ | 0.5000 | 13 | 0.141 9 | 0.125 7 | 20 | 0.159 9 | 0.148 6 |
| $\frac{9}{16}$ | 0.5625 | 12 | 0.182 | 0.162 | 18 | 0.203 | 0.189 |
| $\frac{5}{8}$ | 0.6250 | 11 | 0.226 | 0.202 | 18 | 0.256 | 0.240 |
| $\frac{3}{4}$ | 0.7500 | 10 | 0.334 | 0.302 | 16 | 0.373 | 0.351 |
| $\frac{7}{8}$ | 0.8750 | 9 | 0.462 | 0.419 | 14 | 0.509 | 0.480 |
| 1 | 1.0000 | 8 | 0.606 | 0.551 | 12 | 0.663 | 0.625 |
| $1\frac{1}{4}$ | 1.2500 | 7 | 0.969 | 0.890 | 12 | 1.073 | 1.024 |
| $1\frac{1}{2}$ | 1.5000 | 6 | 1.405 | 1.294 | 12 | 1.581 | 1.521 |

1.

Appendix

1. The settings that were used during the experiments were used to ensure consistency in data collection.

| | | | | |
|---|---|---|----------|--|
| Setup Details | | RCS | | |
| Platform | xWR16xx | Desired Radar Cross Section (sq. m) | 3 | |
| SDK version | 2.0 | Maximum Range for desired RCS (m) | 67.916 | |
| Antenna Config (Azimuth Res - deg) | 4Rx,2Tx(15 deg) | RCS at Max Unambiguous Range (sq. m) | 0.000277 | |
| Scene Selection | | Console Messages | | |
| Desirable Configuration | Best Range Resolution | Done mmwDemo:/>clutterRemoval -1 0 Done | | |
| Frequency Band (GHz) | 77-81 | mmwDemo:/>calibDcRangeSig -1 0 -5 8 256 Done | | |
| Frame Rate (fps) | 1 to 30 | mmwDemo:/>extendedMaxVelocity -1 0 Done | | |
| Range Resolution (m) | 0.039 to 0.043 | mmwDemo:/>bpmCfg -1 0 0 1 Done | | |
| Maximum Unambiguous Range (m) | 3.86 to 11.48 | mmwDemo:/>lvdStreamCfg -1 0 0 0 Done | | |
| Maximum Radial Velocity (m/s) | 0.19 to 0.69 | mmwDemo:/>nearFieldCfg -1 0 0 0 Done | | |
| Radial Velocity Resolution (m/s) | 0.05 | mmwDemo:/>compRangeBiasAndRxChanPhase 0.0 1 0 1 0 1 0 1 0 1 0 1 0 1 0 1 0 1 0 Done | | |
| Plot Selection | | | | |
| <input checked="" type="checkbox"/> Scatter Plot | <input type="checkbox"/> Range Azimuth Heat Map | mmwDemo:/>measureRangeBiasAndRxChanPhase 0 1.5 0.2 Done | | |
| <input checked="" type="checkbox"/> Range Profile | <input type="checkbox"/> Range Doppler Heat Map | mmwDemo:/>CQRxSatMonitor 0 3 6 111 0 Done | | |
| <input type="checkbox"/> Noise Profile | <input checked="" type="checkbox"/> Statistics | mmwDemo:/>CQSigImgMonitor 0 95 4 Done | | |
| Open in Browser | | | | |

2. The first mounting situation was used to keep a constant height and angle when testing distances for the radar.



Stat Calculations and Data

[3]

<https://docs.google.com/spreadsheets/d/1d9carHeEhfIdqGlTqzC2-eMKkJLzBxhSSMgi7bNA2bw/edit?usp=sharing>

Control Group

[4]

| Distance (ft) | Parameter | Mean | SD | CI ± | Lower Bound | Upper Bound |
|------------------|-----------|--------|-------|-------|----------------|----------------|
| 5 | Loc P1 | 5.271 | 0.166 | 0.412 | 4.86 | 5.68 |
| | Loc P2 | 6.037 | 0.197 | 0.489 | 5.55 | 6.53 |
| | Mag P1 | 114.87 | 2.52 | 6.27 | 108.6 | 121.1 |
| | Mag P2 | 108.87 | 5.28 | 13.13 | 95.7 | 122 |
| 10 | Loc P1 | 10.302 | 0.34 | 0.84 | 9.46 | 11.14 |
| | Loc P2 | 11.056 | 0.28 | 0.7 | 10.36 | 11.76 |
| | Mag P1 | 107.13 | 6.3 | 15.7 | 91.4 | 122.8 |
| | Mag P2 | 112.27 | 3.45 | 8.57 | 103.7 | 120.8 |
| 15 | Loc P1 | 14.851 | 0.15 | 0.38 | 14.47 | 15.23 |
| | Loc P2 | 15.639 | 0.14 | 0.36 | 15.28 | 15.99 |
| | Mag P1 | 86.93 | 5.05 | 12.55 | 74.4 | 99.5 |
| | Mag P2 | 95.13 | 5.91 | 14.7 | 80.4 | 109.8 |
| 20 | Loc P1 | 19.313 | 0.14 | 0.35 | 18.96 | 19.66 |
| | Loc P2 | 20.057 | 0.1 | 0.25 | 19.81 | 20.31 |
| | Mag P1 | 89.6 | 2.02 | 5.02 | 84.6 | 94.6 |
| | Mag P2 | 95.13 | 3.34 | 8.16 | 87 | 103.3 |

$CI = \bar{x} \pm t_{0.975} * \frac{s}{\sqrt{n}}$ where n=3 and t=4.303 for CI= 95% with 2 degrees of freedom.

[5]

| Distance (ft) | SD Loc P1 (ft) | SD Loc P2 (ft) | SD Mag P1 (dB) | SD Mag P2 (dB) | Percent Error (%) |
|---------------|-------------------|-------------------|-------------------|-------------------|----------------------|
| 5 | 0.166 | 0.197 | 2.52 | 5.28 | 5.4 |

| | | | | | |
|----|------|------|------|------|---|
| 10 | 0.34 | 0.28 | 6.3 | 3.45 | 3 |
| 15 | 0.15 | 0.14 | 5.05 | 5.91 | 1 |
| 20 | 0.14 | 0.1 | 2.02 | 3.34 | 1 |